Westfälische Hochschule
Gelsenkirchen Bocholt Recklinghausen
University of Applied Sciences

FACHBEREICH ELEKTROTECHNIK UND ANGEWANDTE NATURWISSENSCHAFTEN
ABTEILUNG MOLEKULARE BIOLOGIE

Impact of Different Registration Methods on MEG Source - Analysis

Einfluss unterschiedlicher Registrierungsmethoden auf die Quellanalyse von MEG Daten

Master Thesis

zur Erlangung des akademischen Grades
Master of Sciences (M.Sc.)
im Studiengang Molekulare Biologie
im Schwerpunkt Bioinformatik

vorgelegt von
Marie Theiß
aus Krefeld

Recklinghausen, 18. Juli 2016

Erklärung

Hiermit erkläre ich, dass die vorliegende Arbeit von mir selbst und nur unter Verwendung der angegebenen Hilfsmittel angefertigt wurde. Eingereicht wird die Masterthesis in dreifacher Ausführung.
Alle Abbildungen wurden selbst erstellt, und es wurde keine inhaltsverändernde Bildbearbeitung vorgenommen.

Der erste Teil dieser Arbeit wurde an der westfälischen Wilhelms-Universität im Institut für Biomagnetismus und Biosignalanalyse unter der Anleitung von Priv.-Doz. Dr. Carsten Wolters durchgeführt. Betreut durch Christophe Grova wurde der zweite Teil dieser Thesis im Institut für Physik an der Concordia Universität in Montreal, Kanada erarbeitet.

Recklinghausen, 18. Juli 2016

Marie Theiß

Betreuer:

1. Gutachter: **Prof. Dr. Heinrich Brinck**

Westphalian University of Applied Sciences
Institute for Bioinformatics and Chemoinformatics
August-Schmidt-Ring 10
45665 Recklinghausen

2. Gutachter: **PD Dr. Carsten Wolters**

University of Münster
Institute for Biomagnetism and Biosignalanalysis (IBB)
Malmedyweg 15
48149 Münster

Acknowledgements

Für die Betreuung und Begutachtung dieser Masterarbeit möchte ich mich bei Heinrich Brinck und Carsten Wolters bedanken. Christophe Grova und Andreas Wollbrink haben zudem durch ihre hilfreichen Anregungen und die konstruktive Kritik maßgeblich dazu beigetragen haben, dass diese Masterarbeit in dieser Form vorliegt.

Es ist nicht möglich, alle Menschen namentlich zu erwähnen, die mich in den letzten Jahren unterstützt und während meines Studiums begleitet haben. Trotzdem gilt diesen Personen mein Dank, weil sie alle meine Launen ertragen haben, ohne dabei die Geduld zu verlieren. Besonders hervorheben möchte Sabine Nixon, wie bereits bei meiner Bachelorarbeit, hat sie die undankbare Aufgabe des Korrekturlesens übernommen und mir damit sehr geholfen.

Meinen Professoren danke ich zunächst für eine sehr gute fachliche Ausbildung. Insbesondere aber auch für die aufmunternden Worte, ohne die ich nicht den Mut gehabt hätte für einige Monate ins Ausland zu gehen.

Zuletzt seien noch diejenigen Personen erwähnt, ohne die es nicht möglich gewesen wäre, diese Arbeit zu schreiben. Mein herzlicher Dank gebührt all denjenigen, die ihre Daten für diese Arbeit zur Verfügung gestellt haben, den Mitarbeitern des Instituts für Biomagnetismus in Münster und ganz besonders all den Mitarbeitern im Labor von Christophe Grova.

List of abbreviations

[EEG]	Electroencephalography
[ERF]	Event-Related Fields
[FBM]	Fiducial Based Matching
[GOF]	Goodness of Fit
[ICP]	Iterative Closest Point
[LPA]	Left Pre-Auricular Point
[MEG]	Magnetoencephalography
[MR]	Magnetic Resonance
[MRI]	Magnetic Resonance Imaging
[MRT]	Magnetic Resonance Tomography
[M_z]	Longitudinal Magnetization
[M_{xy}]	Transverse Magnetization
[NAS]	Nasion
[PSP]	Postsynaptic Potential
[RPA]	Right Pre-Auricular Point
[RV]	Residual Variance
[SBM]	Surface Based Matching
[SinSh]	Single Shell
[SinSp]	Single Sphere
[SQUID]	Superconducting Quantum Interference Device

Table of contents

Part I: Impact of Different Registration Methods on MEG Source Analysis

I. Summary

For this thesis the impact of different forward model errors on MEG source localization was evaluated. For this purpose, source localization of somatosensory evoked potentials was performed. Two different head models were used for forward modelling. Moreover, two different approaches to aligning the MRI data to the MEG head coordinate system were used. Since the permeability profile for MEG is almost uniform within the whole head, a basic single sphere head model was used. The second one was a single shell volume conduction model, which submits a simple and fast MEG forward computation for a realistically shaped surface of the brain. This head model should supply more accurate results than the single sphere model. Although the single sphere head model does not fit the brain surface perfectly, the Euclidian distances between the dipole localizations obtained with the different head models were very slight. In most cases they shifted less than 5 mm. Considering this, the single sphere model seems to produce acceptable results for somatosensory evoked potentials. This statement applies independently of the used co-registration method.

Two different co-registration procedures were used to calculate the transformation matrix which specifies how to align the MRI data to the MEG head coordinate system: on the one hand, a frequently used approach which relies on three anatomical markers, and on the other hand, a more advanced procedure which uses the iterative closest point algorithm. In order to depict the differences caused by the method, the Euclidian distance between the localized sources and the shift along the three space dimensions were noted. The Euclidian distance between the reconstructed sources ranged from 4.01 to 16.76 mm. This means that erroneous MRI and MEG data co-registration causes MEG gradiometer sensor positions displacement and therefore affects source localization results. In conclusion, the results show that an accurate knowledge of the MEG gradiometer sensor position relative to the head is necessary to reconstruct neuronal activity for MEG measurements.

I.I *Zusammenfassung*

Diese Thesis untersucht die Auswirkungen verschiedener Fehler im *Forward Model* auf die Quellenrekonstruktion von MEG Daten. Zu diesem Zweck wurden die somatosensorischen Potentiale verschiedener Probanden ausgewertet. Das *Forward Model* wurde für zwei verschiedene Kopfmodelle und mit Hilfe unterschiedlicher Registrierungsmethoden für die MEG und MRI Daten erstellt. Aufgrund der Tatsache, dass die Ausbreitung der magnetischen Felder im Kopf nahezu uniform ist, wurde einerseits ein *single sphere* Kopfmodell verwendet. Das zweite Kopfmodell war ein realistisch geformter Volumenleiter, welcher die Oberfläche des Gehirns repräsentierte. Das *single sphere* Kopfmodell stellt die Geometrie des Gehirns nicht optimal dar. Trotzdem sind die Distanzen zwischen den mittels der unterschiedlichen Kopfmodelle ermittelten Dipolpositionen nur sehr gering. In den meisten Fällen sind die Quellen weniger als 5 mm voneinander entfernt. Diese Ergebnisse lassen darauf schließen, dass das *single sphere* Modell für somatosensorische evozierte Potentiale akzeptable Resultate erzeugt. In diesem Kontext ist nicht entscheidend, welche Registrierungsmethode angewendet wird.

Zur Berechnung der Transformationsmatrix, welche die MRI Daten mit dem MEG Kopf-Koordinatensystem aligniert, wurden zwei verschiedene Registrierungsverfahren genutzt.

Einerseits ein häufig verwendeter Ansatz, der über die Identifizierung dreier anatomischer Marker funktioniert und andererseits ein genaueres Verfahren, bei dem der *iterative closest point algorithm* für die Co-Registrierung genutzt wird. Zur Quantifizierung der durch die Registrierungsmethode verursachten Effekte diente die euklidische Distanz zwischen den rekonstruierten Dipolen. Zusätzlich wurde die Verschiebung der Dipole entlang der einzelnen Raumkoordinaten betrachtet. Der Abstand zwischen den rekonstruierten Quellen variierte zwischen 4.01 und 16.76 mm. Diese Ergebnisse zeigen, dass eine ungenaue Co-Registrierung der MRI und MEG Daten eine fehlerhafte Lokalisierung der MEG Gradiometer Sensoren verursacht. Infolgedessen werden auch die Positionen der rekonstruierten Dipole beeinflusst. Zusammenfassend konnte gezeigt werden, dass es notwendig ist, die Position der MEG Gradiometer Sensoren relative zum Kopf des Probanden genau zu bestimmen, um neuronale Aktivitäten zu lokalisieren.

II. Introduction

This chapter presents a general overview of biological, biophysical and mathematical basics applied in the research. Initially, it gives a brief introduction to the anatomical and biological background of functional brain research. Afterwards different types of neurophysiological data will be introduced. The focus will be upon magnetic resonance imaging (MRI) and magnetoencephalography (MEG). At the end, this chapter gives a brief overview of mathematical methods which are necessary to reconstruct the biological signal from neurophysiological measurements.

II.I *General Organization of the Cerebral Cortex*

The cerebral cortex, also referred to as gray matter, is the outer layer of the brain. It is about 2-3 mm thick and deeply wrinkled, so it contains sulci (depression or fissure in the brain surface) and gyri (ridge on the cerebral cortex). The gray matter is built up of six layers of nerve cells. In general, the cerebral cortex is divided into the left and right hemisphere which are connected by the corpus callosum, a band of nerve fibres. Furthermore, it is possible to define various regions of the cerebral cortex with regard to anatomical localization, function, or cytoarchitectonic criteria.

Four anatomical regions are distinguished, the four lobes:

Table 1| Term, location and function of the anatomical regions of the cerebral cortex.

Lobe	Location	Function
Frontal	At the front of each hemisphere, behind the eyes	Decision making, planning, problem solving
Parietal	Behind the frontal lobe, at the top of the brain	Reception and processing of sensory information
Temporal	Behind the frontal lobe and below the parietal lobe, on both sides of the brain	Memory, emotion, hearing, language
Occipital	At the back of the brain	Vision

Moreover, the cortex can be divided into functional regions, called cortical regions. The association cortices (prefrontal cortex, inferior-temporal cortex and parietal-temporal-

occipital cortex) are not related to motoric or sensory functions. These regions receive signals from different cortical and subcortical areas. Secondly, there are primary and secondary regions related to sensory input (vision, hearing and somatic sensation).

Lastly, the gray matter is parted into the neocortex and the allocortex, with regard to cytoarchitectonic criteria. While the allocortex is built up of three to four layers, the neocortex contains six layers, each with typical cells and fibres [Schmidt1990].

Table 2|Layers of the neocortex and typical cells.

I	Molecular layer	Contains very few neurons
II	External granular layer	Tightly packed small neurons and pyramidal cells
III	External pyramidal layer	Pyramidal cells
IV	Internal granular layer	Stellate cells
V	Internal pyramidal layer	Large pyramidal cells
VI	Fusiform layer	Fusiform cells

II.II *Brain Signal Transduction*

Signal transduction between neurons occurs in terms of electrical transmission. A polarity change across the cell membrane results from an action potential at the axon hillock. The action potential expands along the axon up to the synapse. These action potentials are very weak and exhibit hardly any temporal summation. Afterwards the impulse is transmitted from the presynaptic to the postsynaptic neuron by neurotransmitters. The transmitters generate a potential change at a postsynaptic receptor which is called postsynaptic potential (PSP). This electrical current may flow from the postsynaptic cell to the environment or reverse, depending on excitatory or inhibitory properties of the neurotransmitter. The postsynaptic neuron can be irritated by different neurons at the same time. This means, the slow postsynaptic currents afford a temporal summation. Provided that a certain threshold value is exceeded by all incoming signals, the postsynaptic cell becomes depolarized (exhibiting) or hyperpolarized (inhibiting). The cortex contains pyramidal cells which have parallel orientation perpendicular to the cortical surface. With regard to this fact, electrical transmission of

impulses can be used to determine the neuronal activity, since the spatial and temporal alignment of PSPs creates measurable dipoles [Martin1991].

Somatosensory Evoked Responses

Almost any peripheral nerve can be stimulated by an electrical impulse which is applied on the skin. If the nerve contains motor fibres, the innervated muscle twitches in response to the stimulus. This means, the external stimulus generates a somatosensory evoked response. In clinical practice the median and posterior tibial nerves are used most frequently. In order to stimulate the median nerve, electrodes are placed at the subject's wrist. The stimulus intensity should have a controlled strength to see a clear thumb movement. Since muscle afferents are activated due to the stimulus, a cortical somatosensory response can be observed in reaction. The potentials are generated from the primary somatosensory cortex, thus localized to the parietal scalp region [Nuwer1998].

II.III *Magnetic Resonance Imaging (MRI)*

There are different high resolution imaging methods available for medical diagnostics and research. Computed tomography and radiography are techniques which use x-rays to generate images of internal structures of the body. While radiography creates a single image, the computed tomography generates 3D representations from cross-sectional images of the body. These imaging methods are used for dental examination, mammography or orthopedic and chiropractic examinations.

In contrast, soft body parts like brain, viscera and tumors are visualized by use of magnetic resonance (MR) imaging (nuclear magnetic resonance imaging). Normally, the magnetic moments of the hydrogen protons are rotated in different directions. The magnetic resonance imaging system creates a magnetic field which temporarily aligns the magnetic moments of the hydrogen protons in the same direction (longitudinal magnetization M_Z) and the same phase. Afterwards a high frequency pulse changes the M_Z orientation by about 90 degrees whereby transverse magnetic field components occur. This transverse magnetization (M_{XY}) can be measured as the MR signal. The density of protons in a volume unit defines the maximum

measurable signal. Depending on the hydrogen content tissues appear bright/white (high hydrogen content) or black (low hydrogen content).

Moreover, the contrast in MRI scans depends on different relaxation times. The M_{XY} abates through longitudinal or transversal relaxation. The time required until the spin reverts to M_Z (longitudinal relaxation) is referred to as T1 time. How fast this process occurs depends on the strength of the external magnetic field and the movement of molecules within the tissue. Following it, the spins are irritable again.

If the activated spins do not evolve their energy to the environment, but exchange their energy, the process is called transverse relaxation. After this decay of the M_{XY}, the spins are not in the same phase anymore. The time which is required for transversal relaxation is called T2 and determines how fast the MR signal decays after excitation. It depends on the tissue; it is not determined by the external magnetic field. The transverse and longitudinal relaxations are not influenced by each other.

Similarly to computed tomography, MRI generates 3D representations from cross-sectional images (tomographic images) of the body. The provided image is built up of units called voxels, a 3D image building block. These cubes do not specify the physical dimensions. For that reason, it is necessary to define a head coordinate system. This specifies the relation between voxel indices and physical dimensions [Weishaupt2006].

II.IV *Magnetoencephalography (MEG)*

Electroencephalography (EEG) and magnetoencephalography (MEG) are non-invasive methods of recording neural activity of the brain. The PSPs of pyramidal neurons, which are located in different cortical layers, cause potential differences on the scalp. EEG reflects summed up PSP of a large number of similarly oriented cortical neurons (pyramidal cells in the neocortex) close to the recording electrode. Volume conduction describes the fact that the EEG signal is distorted and blurred by the different conductive properties of the tissues between the recording electrode and the source of the PSP. The EEG signal does not leave the head, therefore the potential is measured on the scalp surface. The MEG is a second electrophysiological technique which records the magnetic field outside the head using an array of superconducting sensors (SQUID, superconducting quantum interference device).

Since the direction of the magnetic field is perpendicular to the velocity of the charge, MEG contains complementary information to EEG. For that reason, MEG is less sensitive to sources generated in gyri (radial sources), as they do not produce a measurable magnetic field outside of the head. In contrast to the electrical current, the magnetic field generated by the electrical current is not influenced by tissue conductivity.

During MEG recordings, the location of the patient's head inside the scanner is determined relative to the MEG sensors. Therefore, three localization coils are fixed to the subject's head (nasion, right and left pre-auricular). The MEG scanner measures the coils and localizes them, in relation to the SQUID positions. The three localization coils are used to define an MEG head coordinate system. It contains the sensor positions, determined with regard to the subject's head [Kringelbach2010].

II.V *Forward Problem*

Reconstruction of neural signals from MEG measurements requires different steps. The forward problem describes how to predict an observation from a theoretical model, if a set of parameters is given. In MEG source analysis this means forecasting the magnetic fields at the sensor level generated by a particular primary source (forward modelling). This problem has a unique solution, since well-defined values of parameters (e.g. geometry of the head, conductivity of tissues, sensor locations) are used. Nevertheless, different forward models produce different solutions. In order to determine the output for a putative source, an individual model of the subject's head is needed. The model contains the geometry as well as the electrical properties of tissues (head modelling). To achieve an accurate forward model, it makes sense to combine highly detailed anatomical information and MEG measurements. For this purpose, a transformation matrix for the co-registration of the MRI voxel to the MEG head coordinates system can be calculated. That way, both data sets are represented within the same coordinate system. Thus, the MEG gradiometer sensor positions are known relative to the subject's head/head model. This is necessary in order to perform a precise forward modelling [Kringelbach2010].

Various types of head models are available. The simplest head model is spherical and does not represent the actual geometry of the head. However, since a single sphere is used to approximate the head shape and a homogeneous conductivity is assumed, an analytic solution is available: the analytical solution of the quasi-static approximation of Maxwell's equations which can be computed to describe the potential on the surface.

A more advanced model is the realistic single-shell volume conduction model. In this case the head is not described as a homogeneous sphere, but as a shell of individual (here the individual brain) shape. This model may produce more accurate results in source reconstruction [Nolte2003].

Maxwell's equations

Maxwell's equations are a set of partial differential equations, which describe the generation of electric and magnetic fields. Moreover, they determine how the fields are altered by charges, currents and each other. In forward computation the equations are used to define the induced electromagnetic fields with regard to the head's tissue and the neural currents.

$$\nabla \cdot D = \rho$$

$$\nabla \cdot B = 0$$

$$\nabla \times E = -\frac{\partial B}{\partial t}$$

$$\nabla \times H - \frac{\partial D}{\partial t} = j$$

The equation introduces several important variables: electric field E, magnetic field B, charge density ρ, current density J, electric displacement field D, magnetic field strength H. Different simplifications and mathematical transformations lead to the following equation for the magnetic flux. It is applicable to each volume conductor model [Nolting2011].

$$B(r) = B_P(r) - \frac{\mu_0}{4\pi}\int_V \sigma(r')\nabla'\phi(r') \times \nabla' \frac{1}{R} dv'$$

Note that a detailed introduction to Maxwell's equation is beyond the scope of this thesis. For further information see [Plonsey1967].

II.VI *Inverse Problem*

The forward problem has a unique solution, while the inverse problem might accept different solutions, depending on the motivation of the experiment. Inverse modelling means to estimate the values of the parameters of the system by the observations made during the experiment. Thereby different objectives or theoretical models might lead to multiple solutions to the same inverse problem. In source reconstruction the PSPs are approximated as single or multiple dipoles. For each dipole 6 parameters (x, y, z location; 2 direction/orientation and strength) are estimated. To perform inverse modelling, it is necessary to solve the forward problem first. Afterwards, a dipole fit can be performed to solve the inverse problem. The method minimizes the error between the forward model solution and the measured magnetic field. For that purpose, the source parameters (location, orientation and strength) of a dipole in the forward model are manipulated until it fits the measured potential or field. At this point it is important to know that in contrast to the orientation and the strength of the dipole, the position is estimated non-linearly [Kringelbach2010].

The sum of squares error is used to calculate the error between the forward model solution and the MEG measurements.

Model for the data:

$$Y_{model} = f(x, a, b, c)$$

Measured potential at each electrode:

$$Y_{measured} = f(x)$$

The equation contains the following variables:

EEG electrode positions: x

Dipole parameters (location, orientation, strength): a, b, c

An optimal dipole is selected by minimizing the sum of squares between the model and the measured potential at each electrode:

$$\min_{a,b,c} \left\{ \sum_{i=1}^{N} \left[Y_{measured,i} - Y_{model,i}(a, b, c) \right]^2 \right\}$$

The squared deviation is needed to determine the residual variance (RV) and maximal goodness of fit (GOF) value for the calculated dipole. These parameters indicate how well the computed dipole describes the measured data.

$$GOF = 1 - RV$$

II.VII *Task*

The MR Tomography (MRT) provides an image of the subject's head with a high spatial resolution. These pictures are useful to determine a dipole position within the subject's brain. They can also be used to construct an individual head model, which provides the tissue geometries and conductivities for source analyses (head modelling). For this purpose, the images need to be pre-processed in mainly two steps. First of all, it is necessary to align the MRI to the MEG head coordinate system (co-registration).

The MR images are usually represented in a 'voxel' coordinate system (voxel space) without physical dimensions. In order to get physical coordinates (coordinates within the source space) for each voxel, a homogenous transformation matrix is needed. This matrix determines the voxel's position within the MEG head coordinate system.

The MEG head coordinate system is based on three anatomical markers. One marker is located at the nasion (NAS) and two at the right and left pre-auricular points (RPA, LPA). The axes are defined in the following way:

Table 3| Axes definition for the MEG head coordinate system.

origin	exactly between LPA and RPA
X-axis	goes towards NAS
Y-axis	goes approximately towards LPA orthogonal to X and in the plane spanned by the fiducials
Z-axis	goes approximately towards the vertex, orthogonal to X and Y

Two different approaches were used to calculate the transformation matrix which specifies how to go from voxel space to the source space. The registration procedures could generate slightly different transformation matrices although both of them should describe the voxel position in the MEG head coordinate system.

A frequently used approach to achieving an accurate co-registration of the MRI to the head coordinate system relies on the three anatomical markers. To determine their positions during the MR recordings, Fiducials (Gadolinium markers) which generate bright spots in the slices are fixed on the subject's head. The markers can be identified manually in the MR images, and the transformation matrix is calculated based on their positions.

In this particular case, an accurate co-registration depends on precise determination of the anatomical markers in both data sets. But this registration procedure contains several possible sources of error, since the landmark digitization has an offset of several millimeters [Singh1997]. Moreover, the Gadolinium markers can slip out of place during recordings. Thus their position cannot be accurately defined within the MRI. Moreover, the MEG scanner does not measure the three localization coils continuously. This means that not every movement of the patient's head is detected. As a consequence, the source space coordinates might differ slightly between MEG and MRI data. Altogether, the small number of landmarks, as well as the sources of error during localization, might lead to an imprecise co-registration of the different data sets.

A second approach uses the iterative closest point (ICP) algorithm to minimize the distance for each point of a point cloud to its nearest neighbor on a surface. A representation of the head surface can be generated by segmenting the MRI into the different tissue types and afterwards creating a triangulated mesh for the scalp. In addition, a point cloud is needed, representing the head surface. It should contain the three anatomical markers, since they are necessary to define the MEG head coordinate system. For this purpose, the ICP algorithm minimizes the distance between the digitized point cloud and the MRI segmented head surface iteratively. A precise determination of the anatomical markers becomes obsolete if the points that represent the surface are used for co-registration. This study determines the sensitivity of MEG source reconstruction for somatosensory evoked fields to the co-registration method with respect to source localization. Considering that, somatosensory evoked responses of 7 healthy subjects were analyzed using a single sphere as well as a single shell head model.

III. Material and Methods

The following section presents an overview of material and data acquisition as well as the methods used for data pre-processing. Data acquisition took place at the Institute for Biomagnetism and Biosignalanalysis of the University of Münster. All processing steps were performed with the Matlab software Toolbox FieldTrip [Oostenveld2011]. The Toolbox offers different algorithms for MEG/EEG and MRI data analysis.

III.I *Data Pre-Processing*

Before source analysis is possible, the different data sets need to be pre-processed. Filtering, cutting the data into interesting segments, and artifact rejection are main steps in MEG data pre-processing. Afterwards the data can be analyzed by averaging. A segmentation step is necessary to extract the outer brain surface from the anatomical MRI scans. This step takes place after MRI – MEG co-registration. Later on, the segmented MRI data are needed to construct an individual head model for forward modelling.

Magnetoencephalography Data

The MEG measurements were made in a magnetically shielded room in supine position. A 275 channel whole head MEG with 29 reference channels (to calculate synthetic gradiometers) (CTF, VSM, MedTech Ltd.) was used to acquire the functional data. Head movements were recorded during the measurements with three head localization coils and the data were discarded if the head movements were greater than 8 mm.

During the recordings a square electrical pulse with 0.5 ms duration was used to stimulate the median nerve of the patient's wrist. In this manner somatosensory evoked potentials were produced. Each run took 7 minutes and included about 950 stimuli with an inter-stimulus interval of 350 to 450 ms. The sampling rate was 1200 Hz. The stimulus took place randomly at the left or right median nerve and its strength was controlled to see a clear thumb movement. The polarity was reversed during the second half of the measurement in order to reduce stimulus artifacts and prevent familiarization.

The raw data from the MEG measurements have to be pre-processed by filtering, re-referencing, baseline correction and identifying artifacts. Moreover, for event-related potential analysis, it makes sense to define data segments of interest and average across trials.

In this manner, the event-related fields (ERF) are obtained and a source reconstruction could be done.

For noise elimination one of the most successful synthetic methods is available: synthetic higher-order gradiometers are computed for cancelling the noise without reducing the signal. Using this noise elimination method, the MEG gradiometers are much more sensitive to the weak brain signals than to sources from the environment.

```
% Synthetic Denoise
cfg.channel = {'MEG' 'MEGREF'};
cfg.gradient = 'G3BR';
rawData = ft_denoise_synthetic(cfg, rawData);
```

Since the data should be analyzed with a view to event-related potentials and fields, it is useful to define the data segments of interest. After the boundaries of those segments have been defined it is possible to represent them as trials. These trials are averaged later to obtain clear signals. Depending on the experiment it is crucial to provide a function which decodes the trigger sequence.


```
% Define Segments of Interest
cfg.trialdef.prestim = 0.1;
cfg.trialdef.poststim = 0.1;
cfg.trialfun = 'trialfunction;
cfg = ft_definetrial(cfg);
trialData = ft_redefinetrial(cfg, rawData);
```

Another step is to identify and remove artificial trials from the data, as they would adulterate the analysis results. Artifacts emerge from eye blinks, muscle contractions or MEG SQUID jumps and could be identified by thresholding the data. The following code shows how MEG SQUID jump artifacts are removable.

```
% Identify and Remove Artifacts
cfg.artfctdef.zvalue.interactive = 'yes';
[cfg, artifact_jump] = ft_artifact_zvalue(cfg);
cfg.artfctreject = 'complete';
cfg.artfactdef.zvalue.artifact = artifact_jump;
cfg = ft_rejectartifact(cfg);
```

In order to get a good signal to noise ratio it is advisable to apply different filters and some additional pre-processing steps to the raw data. For example, the notch filter is useful to remove line voltage frequency (50 Hz) and its harmonics. In addition, a bandpass filter and a baseline correction could be applied to achieve clear data and remove background noise.

```
% Apply Filters
cfg.bsfilter = 'yes';
fg.bpfilter = 'yes';
cfg.demean = 'yes';
cfg.baselinewindow = [-0.075 -0.025];
avgData = ft_preprocessing(cfg, data);
```


The pre-processed trials from the same condition (left or right trigger/ wrist stimulation) can be averaged by timelockanalysis. Afterwards there are different functions available to plot the average.

```
% Timelockanalysis
cfg.trials = (avgData.trialinfo==1);
avgDataTrial1 = ft_timelockanalysis(cfg, avgData);
```

In a butterfly plot, all channels are plotted on top of each other. It can be useful to identify peaks and evaluate data quality. A topo plot depicts the topographic distribution over the head. In this way, event-related potentials become visible for a given latency.

Magnetic Resonance Imaging Data

A T1-weighted (T1w-) MRI scan was acquired for each subject. For this purpose, a 3 Tesla scanner (SIEMENS, Prisma Fit) was available. A 3D-T1w gradient-echo pulse sequence with inversion prepulses, TR/TE/TI/FA= 2.3 ms/3.51 ms/ 1100 ms/ 8°, water selective excitation and cubic voxels with 1 mm edge length was used. During the MR recordings, Gadolinium markers were placed at the nasion (NAS) and at the pre-auricular points (right: RPA, left: LPA). These markers generate bright spots in the MR images. This way, their position can be determined and identified manually within the slices.

The MR images were aligned to the MEG head coordinate system in two different ways. A rigid transformation matrix was calculated, using the positions of the Gadolinium markers during the MRI recordings. Their position was aligned to the head localization coils inside the MEG. In this case, the co-registration relies on matching three anatomical landmarks (fiducials), which are identified in both coordinate systems.


```
% Registration with Fiducials
cfg = [];
cfg.method = 'interactive';
mri = ft_volumerealign(cfg, mri);
```

This frequently used approach will be called *fiducial based matching* (FBM) in the following.

For the second method a surface digitization was performed using a Polhemus digitizer. The positions of 74 electrodes (10-10 system) of an EEG sensor configuration as well as the region around the eyes and the nose were recorded. Furthermore, the digitized head points include the fiducials, positioned at the head localization points inside the MEG. Moreover, the scalp surface was segmented by the individual MR images. The ICP algorithm was used to calculate a transformation matrix which minimizes the distance between the digitized head points and

the MRI segmented head surface. Consequently, this co-registration method uses two individual surface descriptions (digitized head points and MRI segmented scalp surface) to achieve an accurate matching. From here on this approach will be called *surface based matching* (SBM).

```
% Registration with ICP
cfg = [];
cfg.method = 'headshape';
cfg.headshape.headshape = digitizedHeadPoints;
mri = ft_volumerealign(cfg, mri);
```

In the following, two sets of MRI scans are distinguished. The first one was co-registered to the MEG data using the FBM co-registration procedure, while the SBM method was used for the second MRI scans. The individual brain surface was segmented by both MRI data sets.

```
% Segmentation of MRI Scans
cfg = [];
cfg.spmversion = 'spm8';
cfg.brainsmooth = 5;
cfg.brainthreshold = 0.5;
cfg.downsample = 1;
cfg.output = 'brain';
segmentedmri = ft_volumesegment(cfg, mri);
```


III.II *Forward modelling*

A head model is needed to compute the potential distribution on the scalp surface for a given source. Several studies have shown that an accurate source localization depends on the quality of this model. Subsequently to the MRI pre-processing steps, two different head models were generated to analyze the MEG data for each segmentation: on the one hand a basic single sphere (SinSp) head model, and on the other hand a realistic single shell volume (SinSh)

conduction model. The head models were created after the brain had been segmented by the anatomical MRI.

The first model uses a set of points, describing the brain surface, to fit a single sphere. The surface points were gained from the segmented MRI scans.

```
% Generate SingleSphere Head Model
cfg = [];
cfg.method = 'singlesphere';
HeadModel = ft_prepare_headmodel(cfg, segmentedmri);
```

For each subject the sphere has an individual radius.

Table 4| Radii of the single sphere models in mm.

Subject	Radius [mm]
I	69.65
II	70.87
III	71.61
IV	69.33
V	75.98
VI	67.60
VII	72.13

The second model is based on *'The magnetic lead field theorem in the quasi-static approximation and its use for magnetoencephalography forward calculation in realistic volume conductors'* published by G. Nolte [Nolte2003]. A simple and fast MEG forward computation for a realistically shaped surface of the brain is possible with this method.

```
% Generate SingleShell Head Model
cfg = [];
cfg.method = 'singleshell';
HeadModel = ft_prepare_headmodel(cfg, segmentedmri);
```

In a next step a lead field is calculated for each head model. For this purpose, the forward problem is solved for many dipole locations on a regular 3D grid. A grid with 2 mm resolution was prepared for this study. Since the MRI and MEG data were co-registered due to MRI data pre-processing, the calculated head models were already aligned to the MEG gradiometer sensor positions. Moreover, the inverse computation data are needed, as they contain information about the channels that should be included in the forward model computation. Thus, the obtained data can be used to solve the forward problem and calculate a lead field. Later on, the lead field is needed to solve the ill-posed inverse problem of source reconstruction inside the brain volume.

```
% Generate SingleShell LeadField
cfg = [];
cfg.headmodel = HeadModel;
cfg.grid.resolution = 2;
[LeadField] = ft_prepare_leadfield(cfg, avgData);
```


In summary, four different forward solutions were calculated for each subject. In the following they are defined as:

Table 5| Head model type and registration method, which were used for the different forward solutions.

Term	Head Model	Co-Registraion
SpF	SinSp	FBM
ShS	SinSh	SBM
ShF	SinSh	FBM
SpS	SinSp	SBM

III.III *Inverse Methods*

Up to this point, the volume conduction models have been constructed and MEG data pre-processing has been completed. Following this, it is possible to model the data with an equivalent current dipole model. The inverse problem aims to reconstruct the underlying current source from non-invasively measured magnetic potentials. For this purpose, the results of a forward simulation are compared to the measured data. Firstly, the previously prepared lead field is scanned with one dipole. Afterwards the selected function performs a

non-linear fit. In that way the location is found where the dipole model explains the measured MEG topography best. The dipole fit is performed for a given time point and optimizes position, orientation and strength simultaneously. The result can be visualized in a figure which contains the dipole and some selected slices of the anatomical MRI.

```
% Performe DipoleFit
cfg = [];
cfg.numdipoles = 1;
cfg.latency = [TimePoint];
cfg.headmodel = HeadModel;
cfg.grid = LeadField;
cfg.senstype = 'meg';
cfg.channel = HeadModel.label;
cfg.elec= GradiometerSensorPositions;
DipoleFit = ft_dipolefitting(cfg, avgDataTrial1);
```

IV. Results

This chapter presents the results which were obtained using the different co-registration methods. Initially, typical results from MEG data pre-processing are depicted. Afterwards the differences in forward modelling, gained after the SFM and SBM, are depicted for some subjects. Finally, the dipole localization differences with regard to the head model and the co-registration procedure are described.

IV.I *MEG – Data Pre-Processing*

The following plot shows the pre-processed MEG data from Subject VII for the second trigger. A characteristic waveform and topography of a somatosensory response are visible. Figure 1 depicts a butterfly plot. All channels are plotted on top of each other, whereby the different components from the somatosensory response become clear. At time 0.000 s an artifact, caused by the stimulation, can be seen. Behind this, the P20, N30 and P45 components occur.

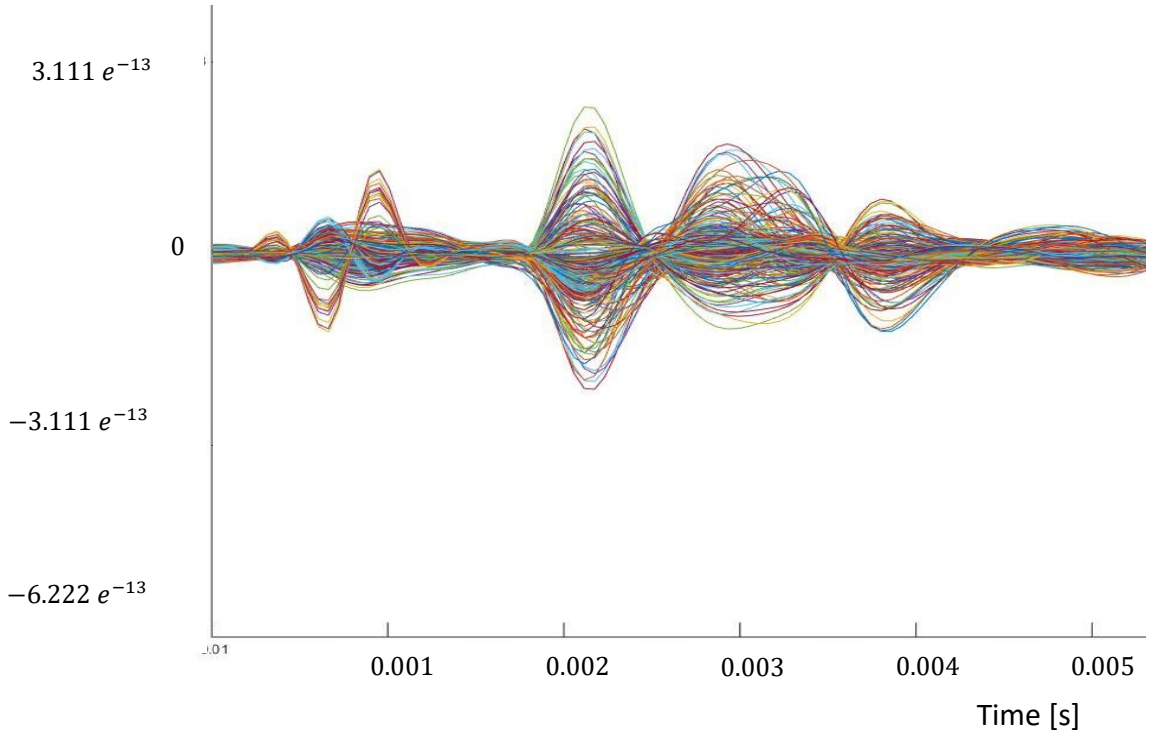

Figure IV-1|Butterfly plot for the pre-processed and averaged MEG data of Subject VII. The plot shows the characteristic waveform of a somatosensory response.

The topographic distribution for a given time point can be shown in a topo plot. The topo plots for the P20 and N30 components are depicted in the following picture.

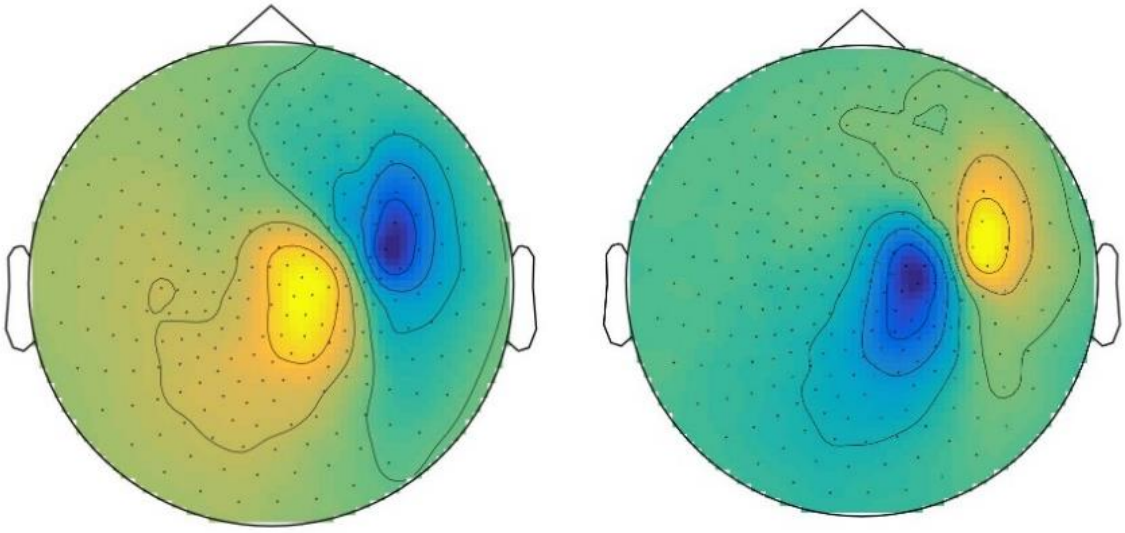

Figure IV-2| Topo plot for the P20 (left) and N30 (right) component of Subject VII. Blue depicts the negative potential and yellow the positive potential.

IV.II *Forward Modelling*

With regard to the co-registration of MRI and MEG data the head model position, relative to the MEG sensor cap, changes slightly. This means that the source reconstruction result is influenced by the co-registration. Since four different forward solutions were calculated, it is possible to investigate two aspects. On the one hand, the head model caused changes can be calculated, and on the other hand, the changes caused by co-registration.

Head Model

Depending on the used head model, different forward solutions are calculated. The following figure shows both head models inside the MEG sensor cap. The SinSh head model is depicted in blue, and the yellow sphere represents the SinSp head model. The MEG gradiometer sensor positions are marked by black points. The figure contains the SinSp and SinSh head model for Subject II and VII obtained after SBM co-registration. It is obvious that the SinSp head model does not fit the brain surface perfectly. The sphere overestimates the brain especially in the temporal region. In contrast, it does not represent the frontal and occipital part of the brain.

The sphere fits the parietal lobe best, which is located behind the frontal lobe, at the top of the brain. This area is responsible for reception and processing of sensory information.

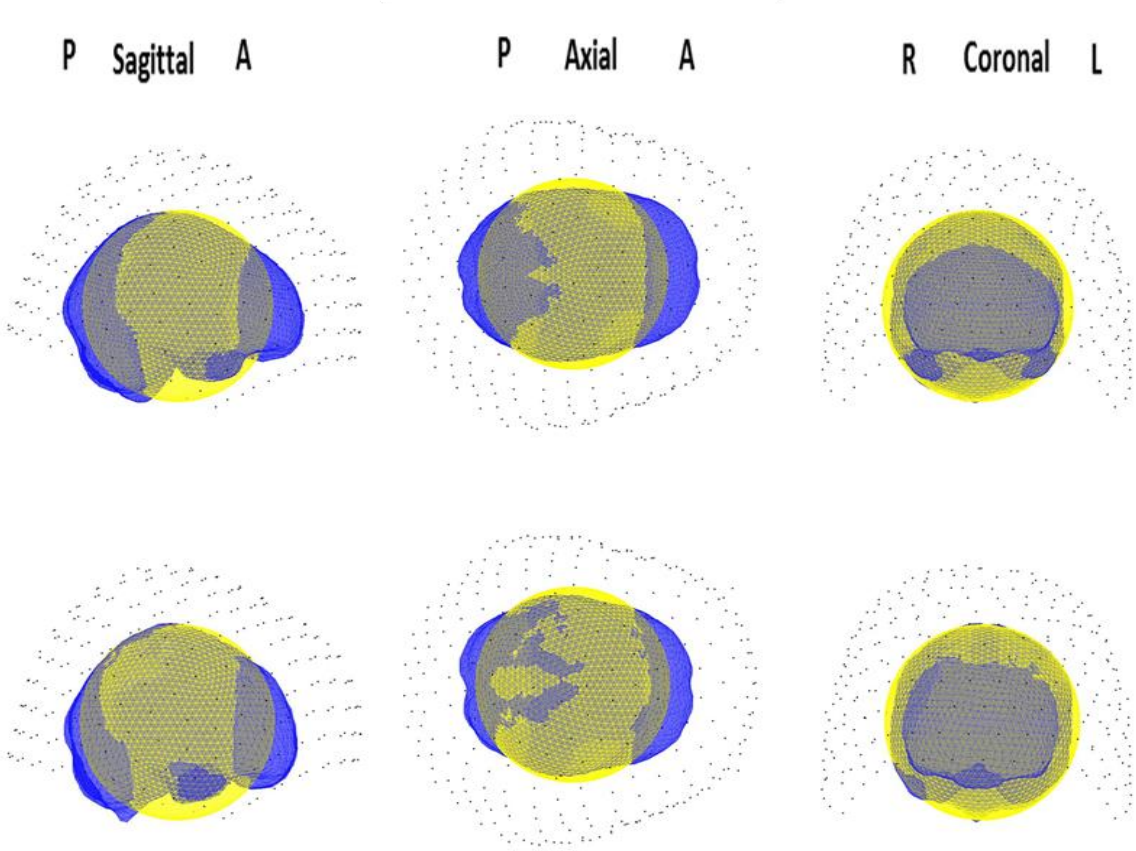

Figure IV-3| Single sphere (yellow) and single shell (blue) volume conductor within the MEG sensor cap (black) for Subject II (upper row) and VII (bottom row) obtained after SBM co-registration.

Registration Method

The first head model used for this study was a SinSp volume conductor. The sphere center is shifted along the three space coordinates, caused by the co-registration procedure. In order to determine the degree of change, the absolute difference of the origins positions is used. The shift along each space dimension as well as the Euclidian distance between the sphere origins are noted in Table 6. These values represent how much the MEG head coordinate system is manipulated.

Table 6| Euclidian distances and shift along the three space dimensions of the single sphere origin positions with regard to the co-registration method. The distances are given in mm.

Subject	Distance	s	c	l
I	**1.93**	0.70	1.75	0.40
II	**8.52**	0.43	1.32	8.41
III	**3.05**	2.62	0.42	1.50
IV	**5.23**	4.95	0.08	1.68
V	**3.61**	2.92	1.04	1.85
VI	**9.15**	8.12	3.50	2.36
VII	**8.45**	0.35	8.39	1.00

Table 7|Mean and Median values for the Euclidian distances and shift along the three space dimensions of the single sphere origin positions with regard to the co-registration method. The distances are given in mm.

	Distance	s	c	l
Mean	**5,71**	2,87	2,36	2,46
Median	**5,23**	2,62	1,32	1,68

As the results show, the SinSp model is mainly shifted along the sagittal axis for 4 subjects (III, IV, V, VI). The largest impact on the coronal axis is visible for Subjects I and VII. Only for Subject II an obvious change along the longitudinal axis occurs. The Euclidian distance between the sphere origins varies from 1.93 to 9.15 mm. For Subject I the changes are less than 2 mm in each direction. On a single occasion (Subject VI) a shift larger 2 mm emerged along two axes. For all other subjects the changes varied from 0.08 to 1.85 mm in two dimensions and shifted more than 2.36 mm along the third one. A difference of more than 8 mm along one axis was observed for the Subjects II, VI and VII. On average a distance of 5 to 6 mm arose between the sphere origins with regard to the co-registration method. The mean shift along each space dimension is about 2 to 3 mm. Nevertheless, it should be noted that the median value is much smaller along the coronal and longitudinal axis.

The co-registration method has the same impact on the SinSh model as on the SinSp model. The following figure depicts the differences caused by the method used for MRI and MEG data co-registration. Obviously, the single shell volume conductor position changes inside the MEG sensor cap with regard to the registration method. The chosen examples are the head models for Subjects II, VI and VII. In this selection, each one illustrates a shift larger 8 mm along one

space coordinate. The red shell represents the head model position obtained after FBM, while the green one was obtained after SBM. The black points mark the MEG gradiometer sensor positions.

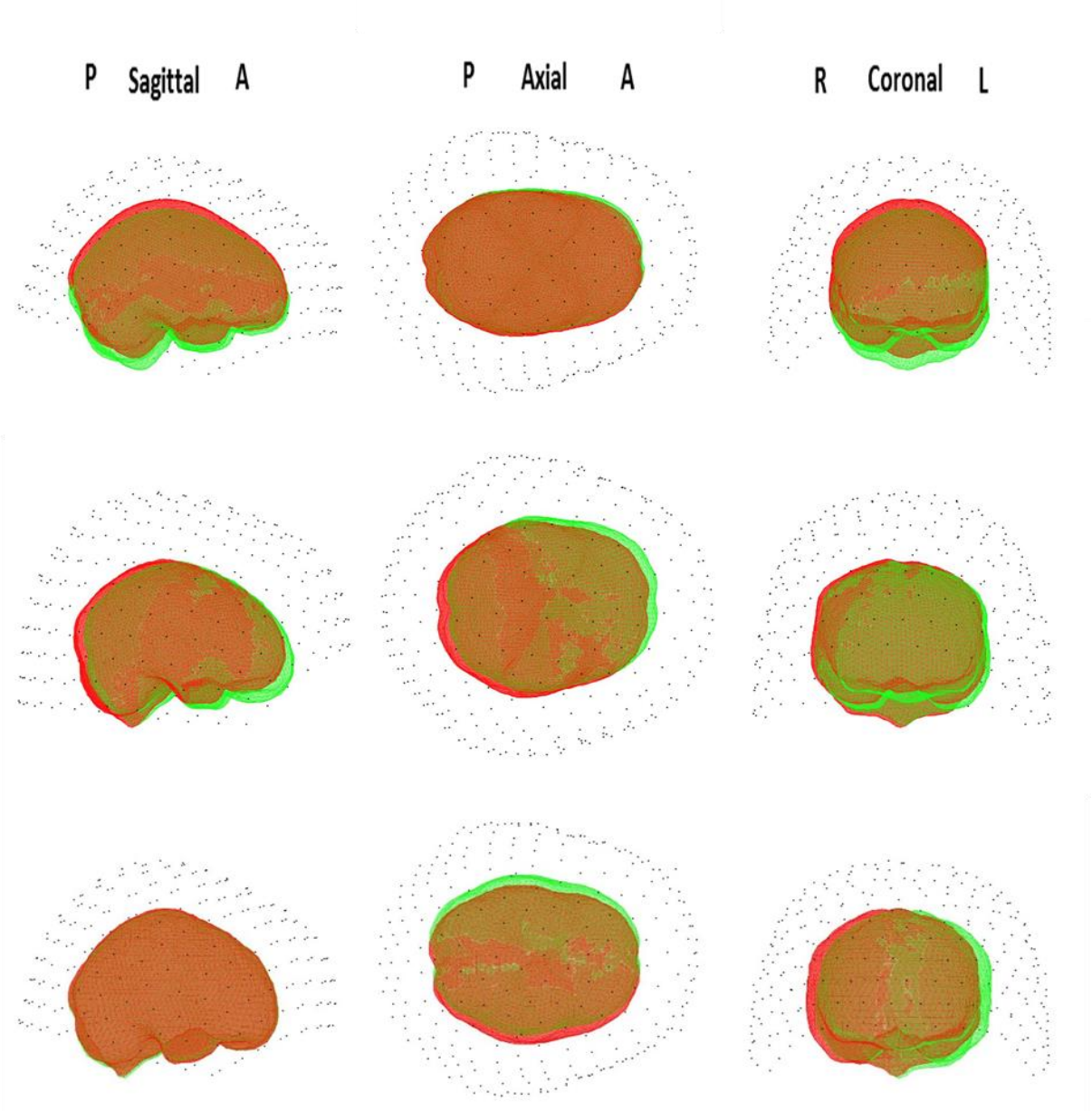

Figure IV-4|Divergent positions of the single shell volume conductor within the MEG sensor cap (black) caused by different registration methods for MRI and MEG data. Red: head model position obtained after FBM registration, green: head model position obtained after SBM registration. Upper row: Subject II; head model is mainly shifted along the longitudinal axis. Middle row: Subject VI; head model is mainly shifted along the sagittal axis. Bottom row: Subject VII head model is mainly shifted along the coronal axis.

IV.III *Inverse Solution*

The inverse solution depends on the forward model. This study considers two different factors, which seem to affect the inverse solution. Changes in dipole localization are traceable to the head model type or to the co-registration procedure. First, the differences in dipole localization caused by the head model are represented. Afterwards, changes caused by the co-registration method are shown. For Subject II two MEG data sets with the same trigger were available. Therefore, the following results for this subject do not contain dipole A, but twice times dipole B (termed IIa and IIb).

Differences Caused by Head Model

Two different head models were used to solve the forward problem. This section shows how much the type of head model influences the dipole localization. Therefore, a dipole fit was performed with each forward model. The dipole localizations obtained with different head models, but identical co-registration methods were compared (SpF compared to ShF and SpS compared to ShS; cf. table 5). The following tables show the shift along each space dimension as well as the Euclidian distance between the dipoles. As reference the SinSh dipole position is used. First the results for the first (left) trigger are depicted and afterwards those for the second (right) one. Each table contrasts the distance obtained with the FBM and the SBM co-registration, respectively. Therefore, they contain the Euclidian distance between the dipoles, as well as the shift along the three space dimensions.

Table 8| Euclidian distances and shift along the three space dimensions of the first dipole position with regard to the different head models for both registration methods. The distances are given in mm.

	FBM				SBM			
Subject	**Dipole A**	**s**	**c**	**l**		**s**	**c**	**l**
I	**4.06**	1.12	-2.90	2.60	**4.12**	1.47	-2.88	2.56
III	**1.14**	0.45	-0.80	0.68	**1.45**	0.13	-0.47	1.36
IV	**3.30**	1.40	-2.36	1.84	**3.20**	1.79	-2.09	1.65
V	**1.09**	1.01	-0.08	0.42	**1.54**	0.94	-0.16	1.20
VI	**5.13**	0.34	-4.88	1.52	**4.98**	1.96	-4.50	0.85
VII	**13.42**	-6.05	-11.75	-2.32	**12.27**	-5.12	-10.38	-4.06

Table 9|Euclidian distances and shift along the three space dimensions of the second dipole position with regard to the different head models for both registration methods. The distances are given in mm.

	FBM				SBM			
Subject	Dipole B	s	c	l		s	c	l
I	**2.66**	1.35	1.82	1.38	**2.76**	1.53	1.64	1.60
IIa	**1.37**	0.19	-0.89	1.03	**1.39**	-0.01	-0.51	1.29
IIb	**0.93**	-0.41	-0.82	0.17	**0.64**	-0.50	-0.40	-0.07
III	**3.01**	0.88	1.23	2.60	**3.18**	1.09	0.94	2.84
IV	**2.82**	1.21	1.75	1.84	**2.89**	0.94	1.53	2.26
V	**2.04**	1.45	0.95	1.08	**2.17**	1.43	0.75	1.46
VI	**1.67**	1.34	-0.22	0.98	**1.57**	0.47	-0.04	1.50
VII	**8.37**	-3.89	7.33	1.04	**10.28**	-5.53	8.29	2.52

The Euclidian distance between the dipole locations varies between 0.64 and 13.42 mm. For most subjects the dipole position changes less than 5 mm with regard to the type of head model. Predominantly the changes along the space directions are smaller than 2 mm. Subject VII constitutes an exception, here the differences are larger than 8 mm. In this case the dipoles are shifted mainly along the sagittal and coronal axes. Overall the dipoles are localized in more superior and anterior positions if a SinSh head model is used. This is not true of the source reconstructions of Subject II and Subject VII. In these cases the dipoles also shift in the other direction. Moreover, in most cases the dipoles are located more laterally, provided the SinSh head model is used. Again Subject II and VI constitute an exception. But in these cases, the dipoles are shifted less than 1 mm along the coronal axis.

The data give some indication whether the co-registration method has an impact on the variation in dipole localization with respect to the head model. There is only one case where the dipole shifts in a different direction depending on the used co-registration method (Subject IIb). The distances between the dipole localization obtained with the different head models are very similar. Thus, the variations between the inverse solution obtained with the SinSp and SinSh head models are hardly altered by the registration method.

Figure 5 displays the dipole locations for the different head models for the second dipole of Subject II (dipole B IIb) and the first dipole for Subject VII, both obtained with SBM co-

registration. The ShS dipole is depicted in blue and the yellow one represents the dipole which was calculated by means of the SpS forward solution.

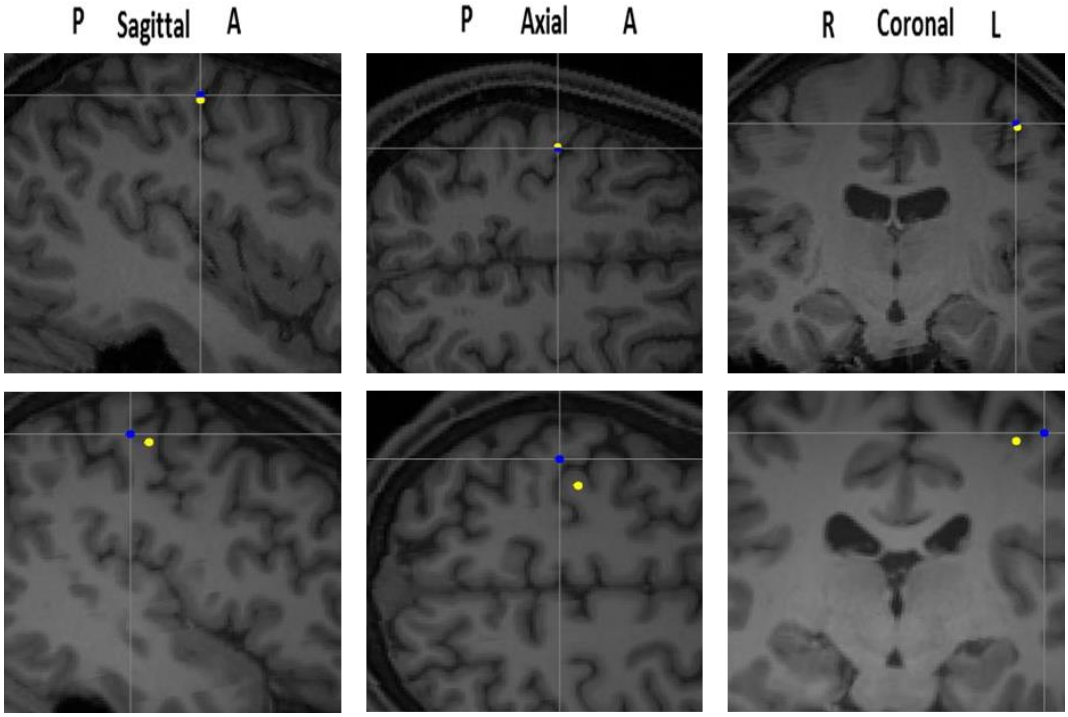

Figure IV-5|Impact of different head models on dipole location for somatosensory evoked fields. The dipole locations for the different head models (yellow: single sphere and blue: single shell) obtained after SBM registration are plotted on T1w-MRI slices. The dipole location based on the single shell was used for MRI slice selection and the other dipole was projected onto these slices. Dipole B for Subjects IIb (upper row) and VII (bottom row).

Differences Caused by Co-Registration Method

With regard to the co-registration method different dipole localizations were calculated. This section illustrates the differences caused by the MRI - MEG data co-registration procedure. For this purpose, the dipole positions, gained with SpF and SpS forward models, as well as those gained with the ShF and ShS forward models are compared to each other. As reference the SBM dipole position is used. Again, one table depicts the results for the left trigger and one those for the right trigger. Each table contrasts the distance obtained with the SinSh and SinSp head model. The Euclidian distance between the localized sources and the shift along the three space dimensions is depicted for all dipoles.

Table 10|Euclidian distances and shift along the three space dimensions of the first dipole position with regard to the different registration methods for both head models. The distances are given in mm.

	SinSh				SinSp			
Subject	Dipole A	s	c	l		s	c	l
I	**5.07**	-3.29	-3.65	-1.24	**5.31**	-3.64	-3.68	-1.2
III	**6.87**	-5.81	0.4	3.63	**6.24**	-5.5	0.06	2.95
IV	**10.47**	-10.28	-0.62	1.9	**10.91**	-10.67	-0.89	2.09
V	**7.04**	-6.2	-2.61	2.06	**6.76**	-6.14	-2.53	1.28
VI	**14.99**	-14.12	-3.66	3.43	**16.76**	-15.74	-4.04	4.11
VII	**12.38**	0.16	-12.07	-2.75	**13.5**	-0.77	-13.44	-1.02

Table 11|Euclidian distances and shift along the three space dimensions of the second dipole position with regard to the different registration methods for both head models. The distances are given in mm.

	SinSh				SinSp			
Subject	Dipole B	s	c	l		s	c	L
I	**4.5**	-0.87	-4.1	1.63	**4.3**	-1.04	-3.93	1.41
IIa	**10.23**	4.84	-0.8	8.97	**10.13**	5.04	-1.17	8.71
IIb	**10.36**	4.76	-0.96	9.15	**10.66**	4.85	-1.38	9.39
III	**6.37**	-6.25	1.09	-0.52	**6.64**	-6.45	1.39	-0.76
IV	**8.02**	-7.75	0.5	2.02	**7.68**	-7.48	0.71	1.6
V	**4.29**	-3.28	-1.73	2.16	**4.01**	-3.26	-1.52	1.77
VI	**9.43**	-8.49	-3.72	1.69	**8.64**	-7.62	-3.90	1.17
VII	**12.61**	-0.74	-11.77	4.45	**13.1**	0.9	-12.73	2.97

Tables 10 and 11 list the Euclidian distances between the dipole locations obtained with the different registration procedures. All results show that the co-registration has a distinct impact on the source localization. The smallest Euclidian distance amounting to approximately 4.0 mm, and the largest difference with a value of 16.76 mm were observed for the SinSp head model. This means, the distance between the reconstructed sources ranges from 4.01 to 16.76 mm with regard to the registration method. In contrast, the distances within the SinSh model vary between 4.29 and 14.99 mm. Nevertheless, it is discernible that the different head models hardly influence the distance between the dipoles. This is reflected by very similar values for the distances caused by the registration procedure within the SinSp and SinSh head model. It should be noted that the Euclidian distances calculated with regard to the head models are smaller than those caused by the co-registration. While the dipole positions changed less than

5 mm for most subjects with the different head model types, the differences caused by co-registration were in most instances larger than 5 mm. Only the first dipole for Subject VII constitutes an exception. Here, the reconstructed sources have a distance of 13.42 mm with regard to the different head models after FBM. But for the SinSh head model the different co-registrations generate a distance of 12.38 mm.

Figure 6 shows the dipole locations for all subjects except for Subject II. The red points represent the dipole locations, obtained after FBM co-registration. The dipole locations after SBM method are depicted as green dots. It can be seen that the red point cloud is located more frontally than the green one. In addition, the green dots seem to be placed in a more lateral position in many cases.

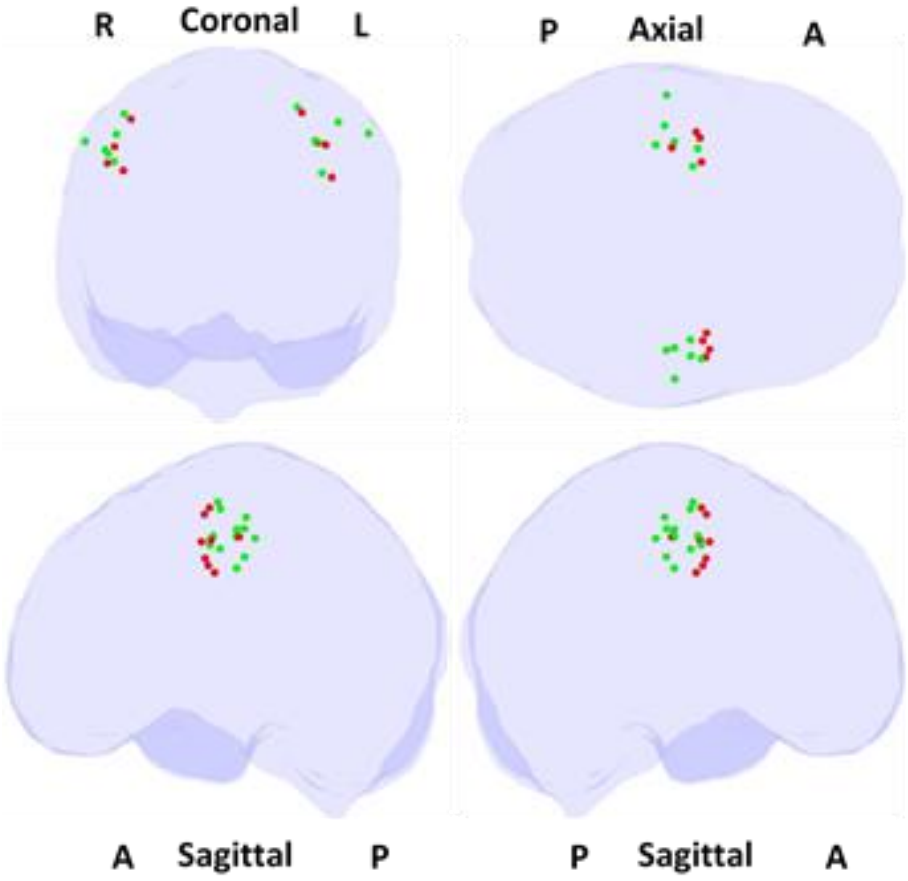

Figure IV-6|Dipole localizations for all subjects, obtained with the different co-registration procedures (red: based on three AL and green: IM). The IM based dipoles are located in more lateral and posterior positions in most cases.

In reference to table 10 and 11 it becomes clear that most dipoles are located in a more posterior position and higher after SBM registration has been applied.

Exceptions are Subjects I, VII (dipole A) and III (dipole B), since those dipoles are located lower. Moreover, the dipoles of Subject II are shifted about 5 mm to the front after the SBM registration procedure (not depicted in figure 6). An obscure effect is visible on the dipoles of Subject VII. In this particular case the dipole shifts in a different direction depending on the used head model. Dipole A is located in a more frontal position in the SinSh head model and in a more posterior position in the SinSp head model when MRI and MEG data have been co-registered by SBM. In contrast it is the other way round for dipole B. This one is located more to the front in the SinSp head model and to the back in the SinSh head model after the SBM registration has been applied. While both dipoles (A and B) were located more laterally with regard to the head model, the co-registration has a different effect. For each subject the sources are shifted in one direction along the coronal axis. In most cases the dipole shifted to the right if the SBM registration method was used. For Subject III both dipoles are located to the left and for Subject IV the dipoles are located more laterally after the FBM has been applied to the MEG and MRI data.

The following figures depict the positions of dipole B for Subjects II, VI and VII. In this manner the distance caused by the registration procedure is illustrated. Again, the red points represent the location obtained after MRI and MEG data were registered by FBM. In contrast, the green points mark the location calculated after SBM of the MRI-segmented scalp surface and the digitized points of the scalp surface. For each example, the dipole is furthest displaced along one space axis. In addition, slight changes along the other two axes are discernible. The first row illustrates the dipoles calculated with the SinSh head model while the second depicts the positions obtained with the SinSp head model. The dipole location based on SBM co-registration was used for MRI slice selection and the other dipole was projected onto these slices. Since the dipole position changes slightly with regard to the head model for Subjects II and VI (see Table 8 and 9) there are hardly any differences between the slices, depicted in the first and second row. In contrast, for Subject VII the head model had a strong impact on the dipole position, which is also visible in the slices.

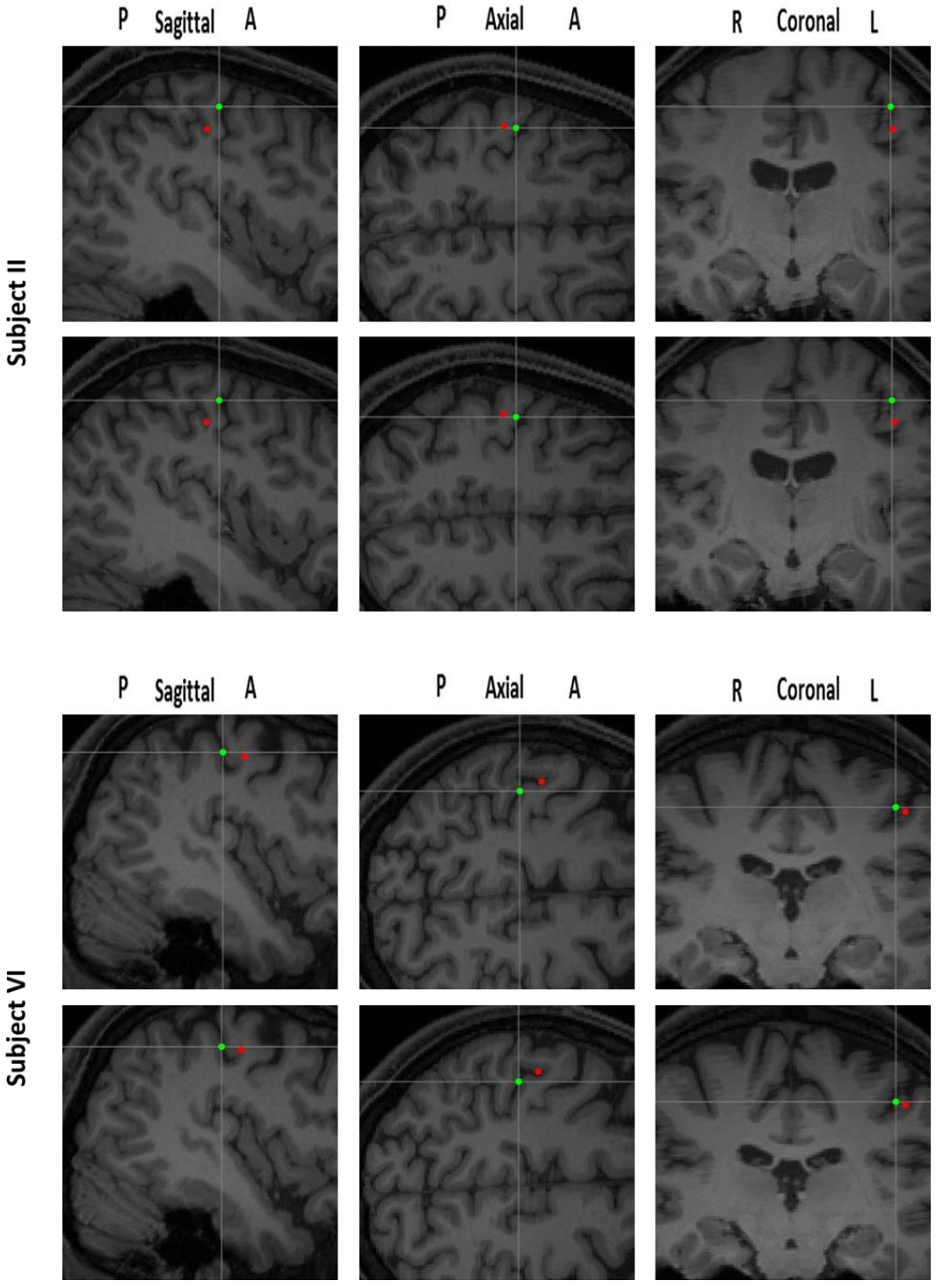
P Sagittal A
P Axial A
R Coronal L
Subject II
P Sagittal A
P Axial A
R Coronal L
Subject VI

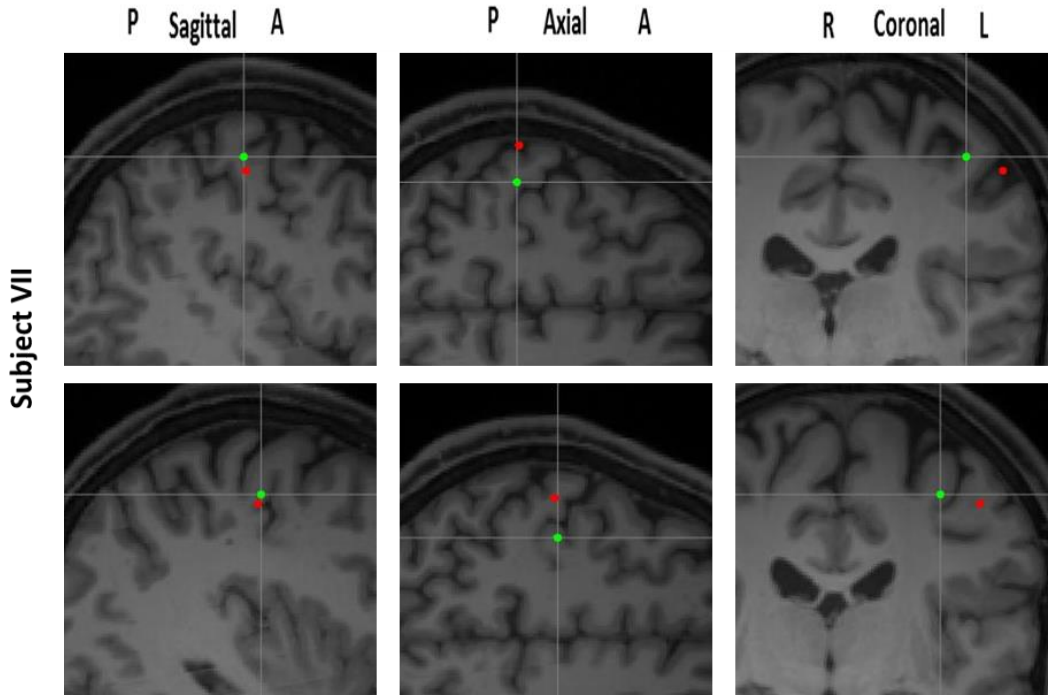

Figure IV-7| Impact of different MEG/MRI co-registration methods on dipole location for somatosensory evoked fields for different subjects. The dipole locations for the different registration methods (red: SBM and green: SBM) are plotted on T1w-MRI slices. The dipole location based on the single shell was used for MRI slice selection and the other dipole was projected onto these slices. The dipoles for both, the single shell head model (upper row) and single sphere head model (bottom row) are depicted.

V. Discussion

A precise forward solution influences the achievable accuracy in the inverse problem. In that regard the impact of forward model errors on MEG source localization was considered in this study. For this purpose, the consequences of different MEG – MRI co-registration methods on source localization of somatosensory evoked potentials were investigated. The co-registration determines the MEG gradiometer sensor positions relative to the head, consequently it has an effect on the forward and therefore the inverse solution. On the one hand the MR images were aligned to the MEG head coordinate system using the positions of three anatomical landmarks (FBM), on the other hand the ICP algorithm was used to calculate a transformation matrix (SBM).

To examine the effect of the co-registration method on the inverse solution the shift in source localization was calculated. Moreover, two different head models were used. In this manner the impact of the co-registration method was matched against the impact of different head model types on the dipole localization. It was shown that errors in MEG gradiometer sensor localization influence source reconstruction more than the type of head model. Apart from one subject, the dipole position changed less than 5 mm with the type of head model. In contrast, the Euclidian distances between the dipole locations obtained with the different registration procedures were larger than 5 mm in most instances. This means that an inaccurate MEG – MRI co-registration leads to mislocalization of reconstructed sources and should be taken into account when working with somatosensory evoked potentials.

Head Models

In a first step, the different head models were compared with each other, since they influence the forward model. Obviously, the SinSp model does not represent the entire individual brain appropriately. Particularly, the temporal, frontal and occipital region of the brain are not approximated properly. However, the parietal lobe is represented quite well. This lobe is located at the top of the brain and has a spherical shape. Somatosensory evoked potentials are processed in the primary somatosensory cortex which is localized to the parietal scalp region. Due to this fact the head model might be sufficient to generate an appropriate forward

model. The SinSh model, on the other hand, is calculated with regard to the individual brain shape, therefore it is supposed to afford a more accurate forward solution.

Section III.III.I presented how the different head models influence the inverse solution. Although the results showed some systematic effects, they were very slight in most cases. *Crouzeix et al.* figured out that a SinSp model causes model-based errors by 2.5 mm and the SinSh model by 2.4 mm for simulated MEG source dipoles in the upper part of the head [Crouzeix1999]. Granted that the measured data exhibit similar errors as simulated data, the results presented by *Crouzeix et al.* are consistent with the perceptions in this study.

The following figure depicts both sources, which were reconstructed for Subject III. It is recognizable that the sources are located next to each other. The dipoles calculated by means of the SpF forward solution are depicted in yellow, while the ShF dipoles are represented in blue. The source locations are plotted on a T1w-MRI slice. The longitudinal and coronal coordinates from dipole B were used for MRI slice selection and the other dipoles were projected onto these slices.

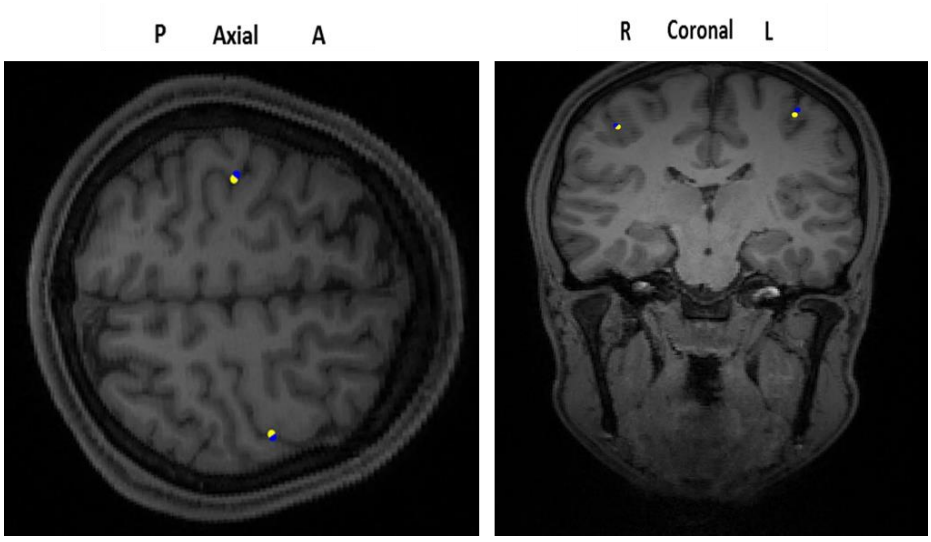

Figure V-1|Subject III. Both dipole locations for the different head models (yellow: single sphere and blue: single shell) obtained after FBM registration. The dipole locations, obtained with the SinSh head model are localized in more lateral and anterior position than the other ones.

It is discernible that the dipoles which were obtained with the SinSh head model are localized more laterally and to the front than the other ones. Besides, a shift upwards can be seen. Nevertheless, the effects are very small. For this reason, the SinSp model seems to be an

acceptable model to reconstruct somatosensory evoked potentials. This outcome was expected, as several studies have shown that MEG is assumed to be less affected by a simplified modelling of the human head [Cho2015].

Additionally, it was examined if the co-registration method changes the impact of the head model. Therefore, the Euclidian distances between the dipoles, obtained after FBM and SBM were applied, can be compared. The distances between the dipoles do not vary much with regard to the registration method. Due to this fact, there is a strong case for believing that the differences caused by the head model are almost independent of the MEG gradiometer sensor positions relative to the head. Admittedly, this statement is restricted to source localization of somatosensory evoked potentials.

Registration Method

The impact of the registration method on the forward model was represented as the degree of change of the SinSp origins positions. It turns out that the head model shifted by 1.93 to 9.15 mm, therefore the coordinates for each MRI voxel within the source space also changed. It should be noted that the head models are shifted along one space dimension predominantly. On average the co-registration method caused a MEG gradiometer sensor positions displacement of 5 to 6 mm. As a consequence, different forward models have been obtained and the sensor displacement influences the inverse solution. The following figure depicts the correlation between displacement of the sphere origin and the effect on the reconstructed source. Therefore, the Euclidian distance between the localized sources and the shift along the three space dimensions is plotted against the change of the SinSp origins positions. Each dot represents the values (of dipole B) for one subject.

In most cases, the more the SinSp origin was shifted, the larger the Euclidian distance between the reconstructed sources. However, this is not true if the individual space directions are taken into account. The dipole might be obviously displaced along one coordinate, although the head model was barely affected in this direction in space by the co-registration method. Take, for example, the case of Subject IIb (sagittal axis) or VII (longitudinal axis).

It has already been taken into account that each sphere origin is mainly shifted along one space dimension. The reconstructed source is also mostly displaced in the same dimension. For the coronal axes and longitudinal axes, the effects seem to be slight in most cases. In contrast, for the sagittal axis the effects differ a lot between the subjects.

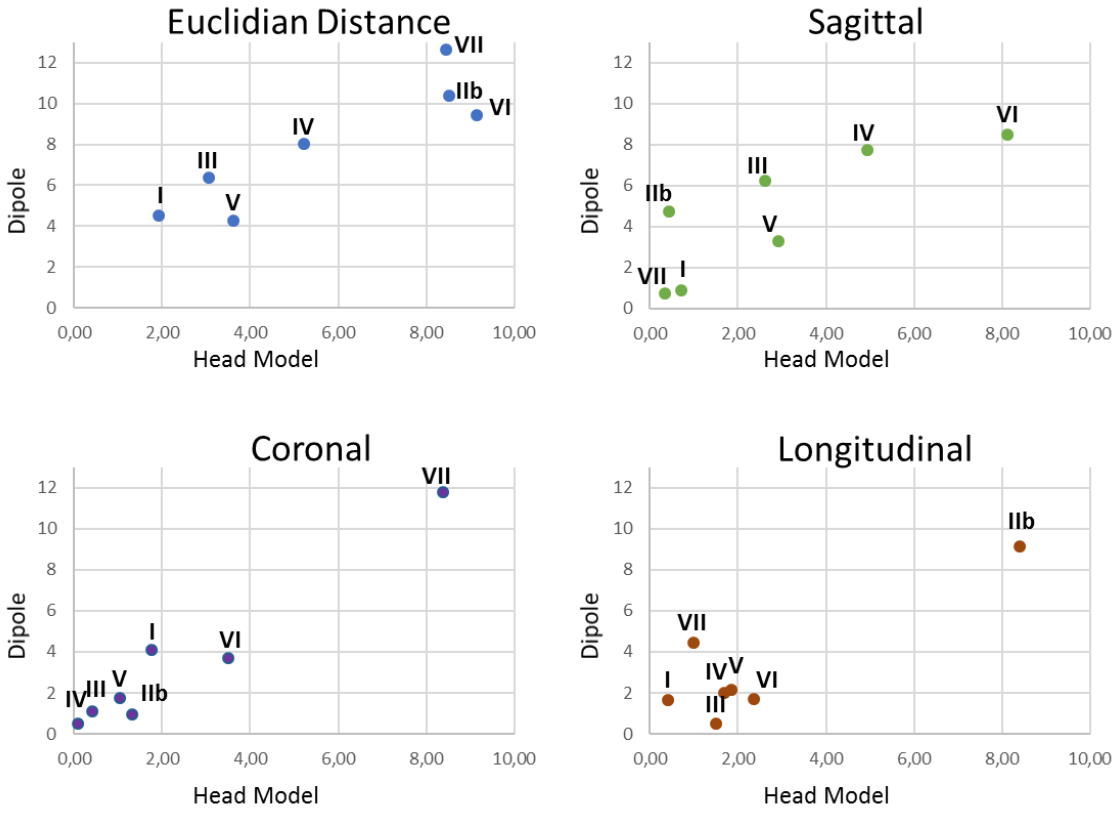

Figure V-2| Correlation between displacement of the sphere origin and the effect on the reconstructed source. The Euclidian distance between the localized sources and the shift along the three space dimensions are plotted against the change of the SinSp origins positions. Each dot represents the values (of dipole B) for one subject. The distances are given in mm.

Previous studies have shown that source localization of somatosensory evoked potentials is barely affected by the type of head model. By contrast, studies dealing with the impact of EEG electrode localization errors on source localization concluded that superficial dipoles are closest to the EEG electrode positions. Therefore, they are most affected by the co-registration method [Zeynep2013].

In this context two types of studies can be differentiated. Firstly, those which examine the effect of random electrode displacement. *Sengül* and *Baysal* reported that an average of 5 mm

EEG electrode mislocalization causes a shift of 4.98 mm in source localization of somatosensory evoked potentials [Sengül2012]. In contrast *Zeynep* and *Scott* shifted the EEG electrode positions in one direction (once 5 mm backwards and once 5 mm to the left). Thereby localization errors up to 12 mm were observed for superficial dipoles. For dipoles in the parietal region a mean error of 6.2 mm (for electrodes shifted backwards) and of 2.6 mm (for left shifted electrodes) was reported. The maximum source localization error was up to 9.1/8.3 mm (for backward/left shifted electrodes) [Zeynep2013].

In this study, the impact of MEG gradiometer sensor positions displacement is taken into account. Section III.III.II represented the effect of co-registration errors on source localization. If the sensor positions shifted up to 5 mm along each axis, a maximum localization error of 8.64 mm (Subject IV) was observed. These results are consistent with those by *Zeynep* and *Scott*, who reported a maximum source localization error of 9.1 mm for superficial dipoles in the parietal region [Zeynep2013]. For those subjects where a shift larger than 8 mm along one space coordinate was detected (Subjects II, VI and VII), the dipoles changed position by up to 13 mm.

This means that MEG gradiometer sensor positions displacement has similar effects on source reconstruction of somatosensory evoked potentials as EEG electrode mislocalization.

VI. Conclusion and Outlook

In this study the effects of different head models and co-registration methods on the MEG inverse problem were examined. Taken as a whole, it was shown that source localization differences, caused by the co-registration method, are larger than those evoked by different head models. A range of studies addressed the importance of head model accuracy for source reconstruction. It became apparent that an accurate volume conductor model is less important for MEG than for EEG forward solutions. The permeability profile for MEG is nearly uniform throughout the hole head (brain, skull, skin), thus simple volume conductor models are sufficient for the forward calculation. With this in view, it is not surprising that the source localizations are hardly affected by the different head models.

As opposed to this, the MEG gradiometer sensor positions have a distinct effect on the reconstructed sources. Previously reported effects of EEG electrode mislocalization on source localization are in accordance with the presented results. This implies that an accurate knowledge of the sensor or electrode positions relative to the head is necessary to reconstruct neuronal activity for MEG or EEG measurements.

Following this thesis it would be interesting to investigate the effect of different co-registration methods on source localizations across the brain space. In this way it would be possible to determine the effect of MEG gradiometer sensor mislocalization in different brain regions. Moreover, an interesting question is, if the co-registration method influences the differences in EEG and MEG source reconstructions. For that purpose, simultaneously acquired MEG and EEG data should be analyzed with respect to the different co-registration methods. Subsequently it would be possible to compare the distances between the dipoles. Possibly, the SBM registration reduces the gap between MEG and EEG source.

VII. Appendix I

VII.I *List of References*

[Cho2015] Cho, J.H.; Vorwerk, J.; Wolters, C.H., and Knösche, T.R. (2015): *Influence of the head model on EEG and MEG source connectivity analysis*.

[Crouzeix1999] Crouzeix, A.; Yvert, B.; Bertrand, O.; Pernier, J. (1999): *An evaluation of dipole reconstruction accuracy with spherical and realistic head models in MEG*. In: Clinical neurophysiology: official journal of the International Federation of Clinical Neurophysiology 110 (12), S. 2176–2188.

[Kringelbach2010] Kringelbach, M.L.; Hansen, P.C.; Salmelin, R. (2010) MEG. An introduction to methods. New York, Oxford University Press. ISBN: 9780195307238.

[Martin1991] Martin JH. *The collective electrical behavior of cortical neurons: the electroencephalogram and the mechanisms of epilepsy*. In: Kandel ER, Schwartz JH, Jessel TM, eds. Principles of neural science. Norwalk: Appleton and Lange, 1991:777–91.

[Nolte2003] Nolte G. (2003) *The magnetic lead field theorem in the quasi-static approximation and its use for magnetoencephalography forward calculation in realistic volume conductors.* Phys Med Biol. 2003 Nov 21;48(22):3637-52.

[Nolting2011] Nolting, W. (2011) *Grundkurs Theoretische Physik 3. Elektrodynamik.* 9., updated Version. Springer-Verlag Berlin Heidelberg, http://dx.doi.org/10.1007/978-3-642-13449-4.

[Nuwer1998] Nuwer, M. (1998) *Fundamentals of evoked potentials and common clinical applications today*. Electroencephalography and Clinical Neurophysiology.

[Oostenveld2011] Oostenveld, R.; Fries, P.; Maris, E.; Schoffelen, J.-M. (2011): *FieldTrip: Open source software for advanced analysis of MEG, EEG, and invasive electrophysiological data.* In: Comput Intell Neurosci 2011, S. 156869. DOI: 10.1155/2011/156869.

[Plonsey1967] Plonsey, R. und Heppner, D. (1967): Considerations on quasi-stationarity in electrophysiological systems. In: *The Bulletin of Mathematical Biophysics* 29.4, S. 657–664.

[Schmidt1990] Schmidt, R.F. and Thews, G.R.A.: *Physiologie des Menschen.* 24. Springer-Verlag Berlin Heidelberg, 1990.

[Sengül2012] Sengül, G.; Baysal, U. (2012): *Determination of measurement noise, conductivity errors and electrode mislocalization effects to somatosensory dipole localization.* In: Biomed Res- India 2012; 23 (4): 518-588. ISSN 0970-938X.

[Singh1997] Singh, K.D., et al. *Evaluation of MRI-MEG/EEG co-registration strategies using Monte Carlo simulation*, Electroencephalogr. Clin. Neurophysio., 1997, 102: 81-85.

[Weishaupt2006] Weishaupt, D.; Köchli, V.D.; Marincek B. (2006) *Wie funktioniert MRI? : Eine Einführung in Physik und Funktionsweise der Magnetresonanzbildgebung,* Springer.

[Zeynep2013] Zeynep, A.A.; Scott, M. (2013): *Effects of forward model errors on EEG source localization.* In: Brain Topography 26 (3), DOI: 10.1007/s10548-012-0274-6.

VII.II *List of Tables and Figures*

Part II: Implementation of a Brainstorm Process for Chamfer Distance based MEG - MRI Co-Registration

VIII. Summary

The following report describes a fully automated surface matching approach for the registration of MEG/EEG and MRI data. The whole method is implemented as a process for the collaborative, open-source application Brainstorm [Tadel2011]. The software offers a flexible plug-in structure, whereby the process function can be run from the Brainstorm interface.

The process is based on the work of Julie Verreault [Verreault2012], who implemented a similar co-registration procedure, which was presented by Schwartz et al. [Schwartz1996]. Moreover, she pointed out which parts should be replaced by tools from the Brainstorm software. In addition to the aspects mentioned by Julie Verreault, the process was modified with a view to improving the results and reducing processing time.

The automatic approach matches two surface descriptions in order to co-register MEG/EEG and MRI data. For this purpose, the skin surface is segmented by the MRI. A binary volume is achieved, which represents the skin surface. Based on this volume a distance transform computation, presented by Borgefors [Borgefors1986], is performed. During this, a map is calculated which contains the distance from the skin surface for each voxel. The second surface description is a 3D point cloud, which represents the skin surface. For the registration process, the distance between the two surfaces (skin surface within the MRI and 3D point cloud) is calculated, using the distance transform volume. In order to minimize the distance between the 3D point cloud and skin surface, extracted by the MRI, a simplex algorithm is used. This algorithm minimizes the mean distance between the two surfaces. Since the algorithm can get stuck in local minima, a reasonable pre-registration is crucial. For this purpose, the surface descriptions are pre-aligned by three anatomical markers. Moreover, the minimization algorithm is launched with several, slightly different, starting points to achieve an optimal result.

Primary simulation studies have shown that the algorithm generates reasonable results. But there are several parameters which might be improved over time. Furthermore, it might be useful to smooth the 3D point cloud, in order to optimize the process.

IX. Introduction

Background information on magnetic resonance imaging (MRI) and magnetoencephalography (MEG) is given in part I of this thesis. Furthermore, the necessity of an accurate co-registration was addressed before. For this reason, these aspects are not taken up again. Instead, this chapter presents the most important aspects of the implemented process. Therefore, the different steps of the automatic co-registration procedure are described.

IX.I *Data Upload*

Before the co-registration procedure can start, the necessary data need to be imported to the MATLAB workspace. The process is launched from the Brainstorm interface, for this reason all data should be available within the Brainstorm database. The process uses an anatomical MRI, a scalp surface and a channel file for a given study. The scalp surface (also called head mask) represents the skin surface and is segmented by the anatomical MRI. It can be generated by Brainstorm and is used to calculate a binary image of the skin. The channel file contains the EEG electrode and MEG gradiometer positions, which should be co-registered to the head surface. The process can use EEG electrode positions or additional head points for the co-registration procedure. If the study does not contain any EEG data, it is crucial to upload additional head points.

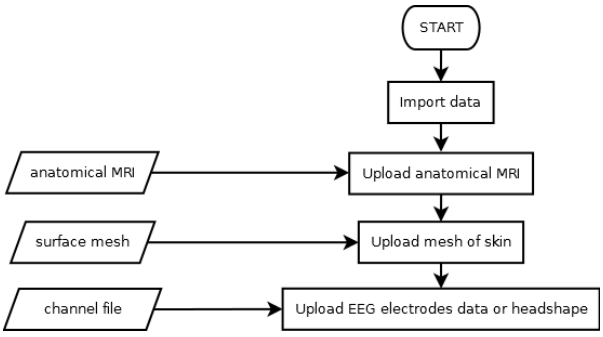

Figure IX-1|Flow diagram of data importation. All data are imported for the Brainstorm database.

IX.II *Distance Transform Computation*

In a second step, the process computes the so-called chamfer volume. This volume represents the distance from each voxel to the skin surface. The method was published by Borgefors in 1986 [Borgefors1986]. The chamfer volume is computed once for a given subject. If there are several studies present for one subject, the distance volume will not be computed again for each study. Instead, the chamfer map which was computed for the first will be imported.

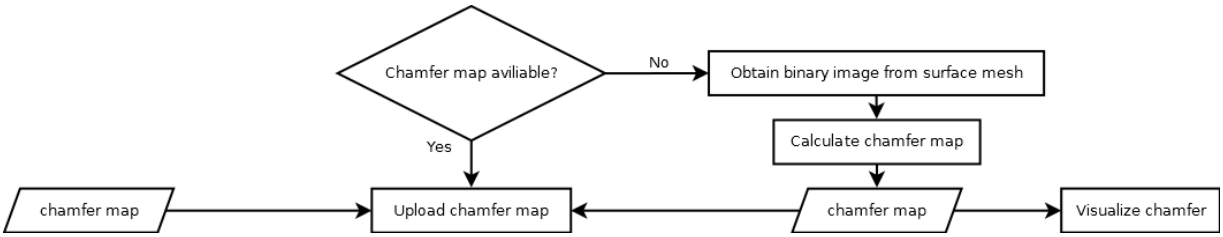

Figure IX-2|Flow diagram of chamfer map computation. The chamfer map is not calculated, if one is available within the Brainstorm database.

The binary image consists of feature (representing the skin surface) and non-feature pixels. The chamfer map represents the distance to the nearest feature pixel for all non-feature pixels. In order to compute these distances in a time-efficient manner the algorithm considers only small neighborhoods. For the given distance map, local neighborhoods of size 3 x 3 pixels are used. This means that the Euclidian distance for each voxel from the skin surface is approximated with the help of a 3 x 3 mask [Borgefors1986].

D1: 3
D2: 4
D3: 5

D3	D2	D3
D2	D1	D2
D3	D2	D3

D2	D1	D2
D1	0	D1
D2	D1	D2

D3	D2	D3
D2	D1	D2
D3	D2	D3

Figure IX-3| Three-dimension chamfer mask of length 3.

IX.III *Minimization Algorithm*

Based on the chamfer distance map, the mean distance between the skin surface and the 3D point cloud is calculated. *Schwartz et al.* reported that the standard deviation associated with the mean distance did not achieve better results than the square mean distance [Schwartz1996]. The square mean distance is defined as cost function, although it is an implicit cost function. In order to minimize this cost function an optimization method is used, which avoids the computation of the derivate. Therefore, an algorithm is needed which searches local minima by using function value evaluations at different positions. While *Schwartz et al.* used the Powell algorithm, the presented process uses a simplex algorithm.

In order to launch the algorithm, a 6D starting point is needed. The vector contains the three translation and three rotation parameters. In the end, the algorithm returns an optimized vector, which contains optimized values for the six motion parameters.

$$\begin{pmatrix} init_{tx} \\ init_{ty} \\ init_{tz} \\ init_{rx} \\ init_{ry} \\ init_{rz} \end{pmatrix} \quad \begin{pmatrix} opt_{tx} \\ opt_{ty} \\ opt_{tz} \\ opt_{rx} \\ opt_{ry} \\ opt_{rz} \end{pmatrix}$$

Figure IX-4| General notation of the input and output vectors for the minimization algorithm.

Depending on the start position, the algorithm might find different local minima and different optimized motion parameters. For this reason, the process uses multiple starting points for the purpose of finding a good local minimum, or even better, the global minimum. Once, the initial pre-registration, based on the three anatomical landmarks (see FBM in part I of this thesis) is used as initial point. The pre-registered point cloud is moved slightly along and around the different space dimensions to create new starting points for the optimization algorithm. By doing so, a local grid search is performed in order to find the global minima. At this point the process starts from 625 different starting points.

$$\begin{pmatrix} -0.0025 \\ 0 \\ 0 \\ 0 \\ 0 \\ 0 \end{pmatrix} \quad \begin{pmatrix} -0.0015 \\ 0 \\ 0 \\ 0 \\ 0 \\ 0 \end{pmatrix} \quad \begin{pmatrix} 0 \\ 0 \\ 0 \\ 0 \\ 0 \\ 0 \end{pmatrix} \quad \begin{pmatrix} 0.0015 \\ 0 \\ 0 \\ 0 \\ 0 \\ 0 \end{pmatrix} \quad \begin{pmatrix} 0.0025 \\ 0 \\ 0 \\ 0 \\ 0 \\ 0 \end{pmatrix}$$

Figure IX-5| Sample set of input vectors. The starting point is translated along the x-axis. Dimensions are in [m].

For each starting point a set of motion parameters is calculated by the minimization algorithm. The set consists of six parameters, three for translation and three for rotation. These parameters are used later on to calculate the transformation matrix. The optimal set of motion parameters is selected, by evaluating the cost function value. The assumption is that the best

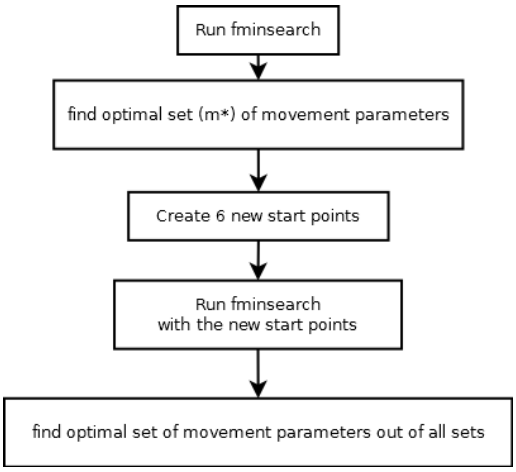

Figure IX-6| Flow diagram of the minimization procedure.

motion parameters generate the smallest cost function.

The optimal set of motion parameters is used to create six additional, random starting points. Each of the six random starting points consists of five random values and one parameter from the optimal parameter set.

$$\begin{pmatrix} opt_{tx} \\ rand_{ty} \\ rand_{tz} \\ rand_{rx} \\ rand_{ry} \\ rand_{rz} \end{pmatrix} \begin{pmatrix} rand_{tx} \\ opt_{ty} \\ rand_{tz} \\ rand_{rx} \\ rand_{ry} \\ rand_{rz} \end{pmatrix} \begin{pmatrix} rand_{tx} \\ rand_{ty} \\ opt_{tz} \\ rand_{rx} \\ rand_{ry} \\ rand_{rz} \end{pmatrix} \begin{pmatrix} rand_{tx} \\ rand_{ty} \\ rand_{tz} \\ opt_{rx} \\ rand_{ry} \\ rand_{rz} \end{pmatrix} \begin{pmatrix} rand_{tx} \\ rand_{ty} \\ rand_{tz} \\ rand_{rx} \\ opt_{ry} \\ rand_{rz} \end{pmatrix} \begin{pmatrix} rand_{tx} \\ rand_{ty} \\ rand_{tz} \\ rand_{rx} \\ rand_{ry} \\ opt_{rz} \end{pmatrix}$$

Figure IX-7|General notation of the new input vectors for the minimization algorithm.

Finally, the final set of motion parameters is selected from all 631 calculated parameter sets. It is checked if the optimization algorithm achieved the maximum number of iteration steps

while calculating this parameter set. In that case, the optimization algorithm is launched once again, using the optimal set of motion parameters as start position.

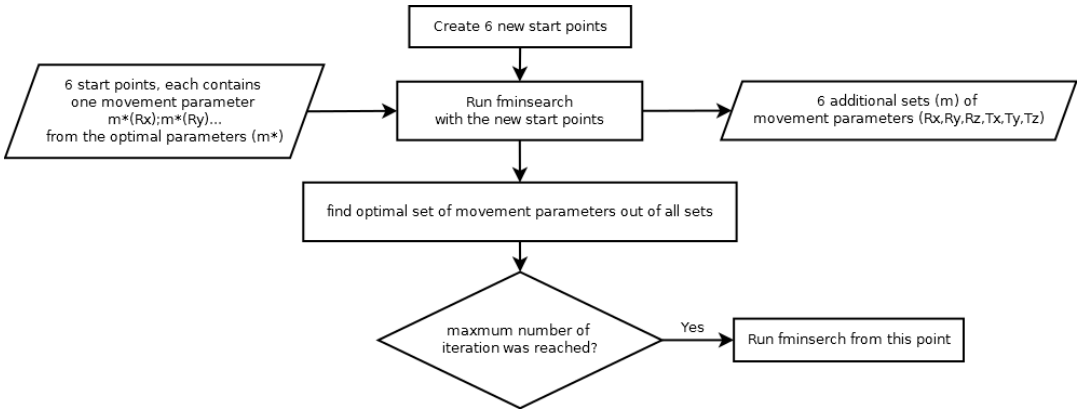

Figure IX-8| Flow diagram of the last optimization steps.

IX.IV *Apply Motion Parameters*

In the end, the process calculates the transformation matrix, which co-registers the skin surface and the 3D point cloud, from the final set of motion parameters. This matrix is used to align the EEG electrodes and MEG sensor positions with the MRI data.

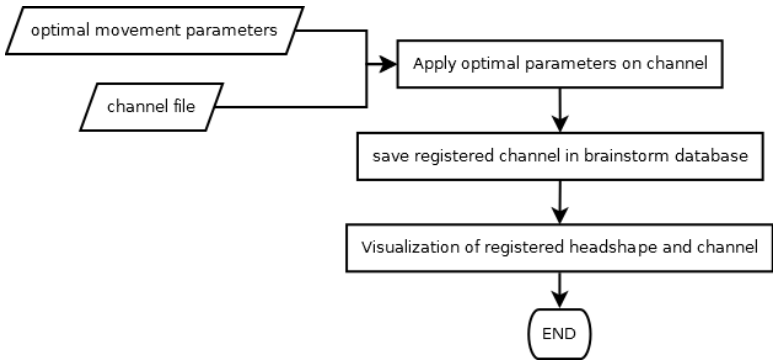

Figure IX-9| Flow diagram of the channel transformation.

The channel positions are transformed, and the channel file within the Brainstorm database is updated. Moreover, the chamfer map, which was calculated in the previous steps, is added to the Brainstorm database before the process stops. Note that the channel file is updated for the given study while the chamfer map is added to the given subject.

X. Material and Methods

This section presents an overview of the structure and the code of the implemented process and the simulation study. The study was used to evaluate the results produced by the process. For the simulation several MATLAB functions were used. The implemented process is available for the open-source application Brainstorm, but it uses functions from different MATLAB toolboxes. A tutorial which describes how the process can be launched from the Brainstorm interface can be found in the appendix.

X.I *Code Structure*

A detailed tutorial on the Brainstorm website describes how a process, which will then be run from the Brainstorm interface, should be implemented. The whole process is saved in a single *.m-file, which contains different functions and methods. The following subsections give a brief overview of the general process structure for a brainstorm process. The main idea for the functions needed for this particular process is outlined in the introduction part. For this reason, the present section focuses on the implementation for the minimization procedure (see section II.III).

Brainstorm Process Functions

The first function (or process function) launches a single script which is part of the Brainstorm software. This script is needed to call the other functions included in the brainstorm process.

```
function varargout = process_AlignChamferDistance(varargin)
                     macro_methodcall;
                                end
```

Three functions are used to set up the process and define input and output arguments. The first function `GetDescription()` returns a structure that describes the process; it defines the following aspects:

s.Process.Comment	process description within the drop-down menu of the Brainstorm interface
sProcess.Category	defines how the process is supposed to behave
sProcess.SubGroup	subgroup, which contains the process
sProcess.Index	relative position, where the process is placed within the drop-down menu of the Brainstorm interface
sProcess.InputTypes	type of input variables (e.g.: raw, data, results, …)
sProcess.OutputTypes	type of output variables (e.g.: raw, data, results, …)
sProcess.nInputs	number of input variables
sProcess.nMinFiles	minimum number of files included in input variables

```
%% ===== GET DESCRIPTION =====
function sProcess = GetDescription() %#ok<DEFNU>
sProcess.Comment = 'Co-Registration using chamfer distance';
sProcess.FileTag = '';
sProcess.Category = 'Custom';
sProcess.SubGroup = 'Import anatomy';
sProcess.Index = 4;
sProcess.InputTypes = {'data'};
sProcess.OutputTypes = {'data'};
sProcess.nInputs = 1;
sProcess.nMinFiles = 1;
end
```


As input argument, a study file folder from the Brainstorm database can be used. The process modifies the contained channel file only, while the functional data are not changed. Additional data, like the anatomical MRI and the head surface, are loaded from the anatomical data which belong to the study subject. The input data need to contain at least one functional data file.

The second function is used to format the comment, therefore it returns a string which identifies the process in the Brainstorm interface.

```
%% ===== FORMAT COMMENT =====
function Comment = FormatComment(sProcess) %#ok<DEFNU>
    Comment = sProcess.Comment;
end
```

The fourth function, which is included in every Brainstorm process, is called in the following way:

```
OutputFile = Run(sProcess, sInputs) %#ok<DEFNU>
```

It executes the process and is, in contrast to the previous functions, not a descriptive one. This means that it imports the input files and performs the co-registration before it returns the output to the Brainstorm database. A main part of this function codes the interaction with the Brainstorm database. Moreover, it includes most of the steps which are crucial for the minimization procedure (explained in section II.III).

The most important step of this procedure is to create a search grid to start the minimization algorithm from different starting points. The pre-registration, based on the three anatomical landmarks, is defined by the initial motion vector:

$$\begin{pmatrix} 0 \\ 0 \\ 0 \\ 0 \\ 0 \\ 0 \end{pmatrix}$$

Figure X-1| Motion vector, which represents the fiducial based co-registration.

Changing one or more of the motion parameters moves the 3D head shape relative to the skin surface and therefore creates a new starting point. In order to create a couple of starting

positions, nested for-loops are used. In each step one motion parameter is changed. By doing so, a search grid with 625 grid points is created. The different starting points are rotated around the z-axis only and not the x- or y-axis.

```
        for tx = [-0.0025 -0.0015 0 0.0015 0.0025]
              for ty = [-0.0025 -0.0015 0 0.0015 0.0025]
                    for tz = [-0.0025 -0.0015 0 0.0015 0.0025]
                        for rZ = [-0.004 -0.002 0 0.002 0.004]
randStart = [tx ty tz 0 0 rZ];
[o,FVAL,EXITFLAG] = fminsearch(minimize,randStart,options);
                        end
                    end
              end
        end
```


The minimization algorithm itself is a simplex algorithm, implemented in MATLAB. As a second step during the optimization procedure, some random starting points are used. These starting positions consist of one optimized motion parameter and five random values, which move the head shape up to 0.00125 m in each direction. The whole registration procedure takes place in the voxel space; for this reason, the head point and EEG electrode coordinates are transformed to the MRI voxel space. Moreover, the physical space dimensions are changed from mm to m.

Sub-Functions

The process function includes several sub-functions. These functions are called from the run function and fulfil different tasks for the process.

Some steps are needed to calculate the chamfer map and add it to the Brainstorm database. To organize these steps, a function which is called `preprocessing_mri` is included in the process. This function uses the full path for the skin surface file, the active anatomical MRI, as

well as the skin surface for the given subject from the Brainstorm database. First of all, the function checks if a chamfer volume is available within the Brainstorm database. If there is no chamfer map present for the given subject, other sub-functions are executed: on the one hand, a function which creates a 3x3x3 mask for the chamfer matrix, and on the other hand, a function called `Chamfer_Map3`. It calculates the chamfer distance map with the mask of 3x3x3. This sub-function returns the required chamfer map. Additional input variables are crucial for the pre-processing function to save this volume within the Brainstorm database. For this purpose, the function `save_chamfer` is used.

There are more sub-functions included in the process. These functions are related to the optimization process. In order to launch the minimization algorithm, a cost function is needed. It calculates the cost for a given registration (set of motion parameters). The cost is defined as the square mean distance between the skin surface and the 3D point cloud. The cost function is used as input (function handle) for the minimization algorithm.

Before the optimized motion parameters can be applied to the head points and the EEG electrode or MEG sensor positions, it is necessary to calculate a transformation matrix. This step is done by the sub-function `M_transform`. The obtained motion matrix is used as input parameter for the `TransformChannel` sub-function. This one changes the Brainstorm channel file by moving the channel positions and changing the MEG sensor orientation.

X.II *Study Design for the Simulation*

A sample data set from the Brainstorm website was used for the simulated study. Using a cluster algorithm, some representative head points were selected from the head surface. These head points were used as EEG electrode positions instead of recorded coordinates. A Gauß-function (mean value of 0 and standard derivation of 1) was used in order to add some noise to the simulated electrode recordings. Moreover, random transformation matrices were applied to move these points from their original position. The representative points were translated up to 5 mm along and 10 ° around each space dimension.

Afterwards the registration process was applied to the data, in order to co-register the simulated EEG electrode positions with the MRI data set. The results were evaluated, by calculating the Euclidian distance between the co-registered EEG electrode positions and their

original position. As an optimal result for this simulation, the co-registration algorithm would return the inverse matrix to the random transformation matrix.

The study included a set of 220 representative head points and various amounts of noise (1 %, 5 %, 10 %, 15 %). Furthermore, the registration process was applied to the data for 50 different random transformations.

XI. Results

The following chapter presents the co-registration results. The co-registration, obtained by use of the implemented process, can be evaluated easily for the simulated study. For this purpose, the Euclidian distance between the original position of the representative head points and their position after co-registration is calculated. Furthermore, some study data were co-registered using the implemented process. In these cases, a visual evaluation of the results is done, since the perfect position for the recorded head points is unknown.

XI.I *Simulated Study Data*

The design for the simulated study is described in section III.II . In order to compare the results to those of a well-working co-registration procedure, another implementation, available in Brainstorm, was used. Both algorithms were applied to the simulated data and afterwards the obtained results for both co-registration procedures were compared to the original positions for the representative head points. In order to find out how much the results are influenced by noisy data, two different values were calculated. On the one hand, the distance between the co-registered head points and the original position, without noise and transformation, and on the other hand, the distance between the co-registered head points and the original position, after the noise had been added to the data, but no transformation had been applied. In the following, boxplots are used to depict the distances, with regard to the amount of noise. The following picture depicts the boxplots for the Brainstorm co-registration. It is visible that a very small co-registration error is achieved for low noise levels. The median Euclidian distance between the re-aligned head points and their original position is less than 0.5 mm. Moreover, there is no evidence that the algorithm overfits the head points, since the distribution of distances between the noisy and the original positions and the re-aligned and original positions are almost identical. For higher noise levels the algorithm produces less optimal results. The distances between the noisy head point positions and the re-aligned head point positions are very similar to those between the original head point positions and the re-aligned head point positions. Nevertheless, the distance between their noisy and original positions is much smaller. For this reason, the algorithm does not fit the simulated EEG electrode positions perfectly to the skin surface.

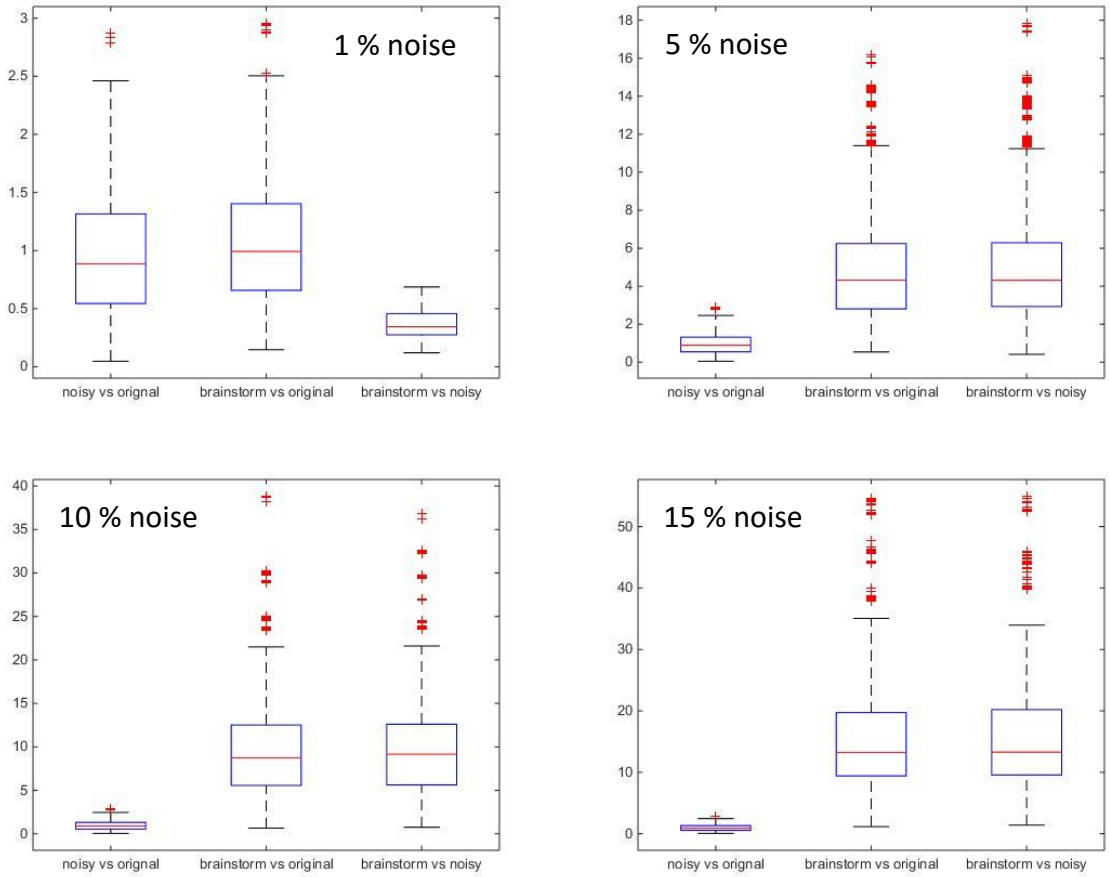

Figure XI-1| Co-Registration results obtained by the original Brainstorm process. Boxplots for the Euclidean distance [mm] between the original and noisy, the original and re-aligned, and the noisy and re-aligned positions of the head points for different noise levels. The process aligns the simulated EEG electrodes almost perfectly to the head surface if the noise level is very low.

For the new co-registration procedure, the boxplots show similar results as for the Brainstorm process, albeit the algorithm shows the same behavior for all noise levels. It should be noted that the Brainstorm process aligns the simulated EEG electrodes almost perfectly to the head surface if the noise level is very low. In contrast, a median distance of approximately 2 mm is observed between the re-aligned head points and the original positions, as well as the noisy head points, after the chamfer based co-registration has been applied to the data.

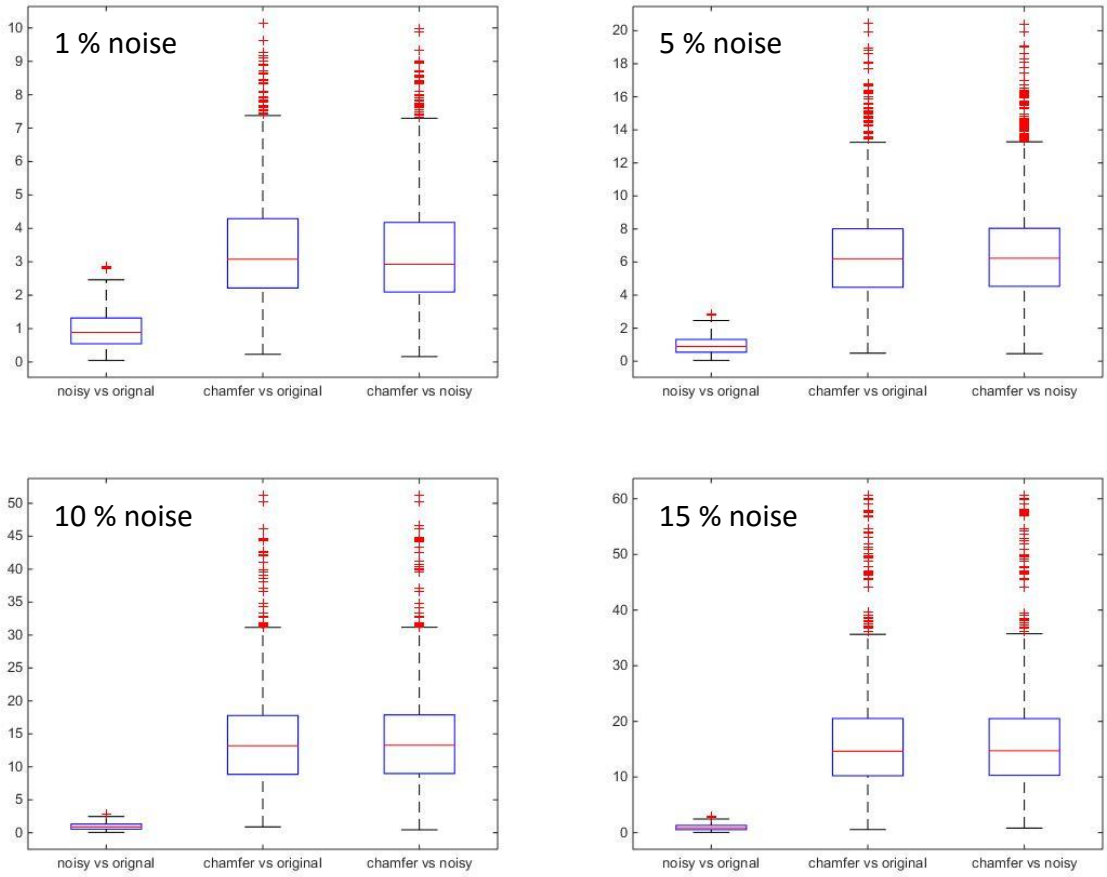

Figure XI-2| Co-Registration results obtained by the chamfer based Brainstorm process. Boxplots for the Euclidean distance [mm] between the original and noisy, the original and re-aligned, and the noisy and re-aligned positions of the head points for different noise levels. The algorithm shows the same behavior for all noise levels.

XI.II *Real Study Data*

In a second step, the Brainstorm process was applied to some real study data. In doing so, it was taken into account if the process was influenced by the noise of study data. The results show that the individual head points were aligned properly to the head surface. However, for two subjects the recorded points do not fit the skin surface all over the head. The point clouds seem to be deformed in the occipital (Subject B) or lateral (Subject A) region of the head.

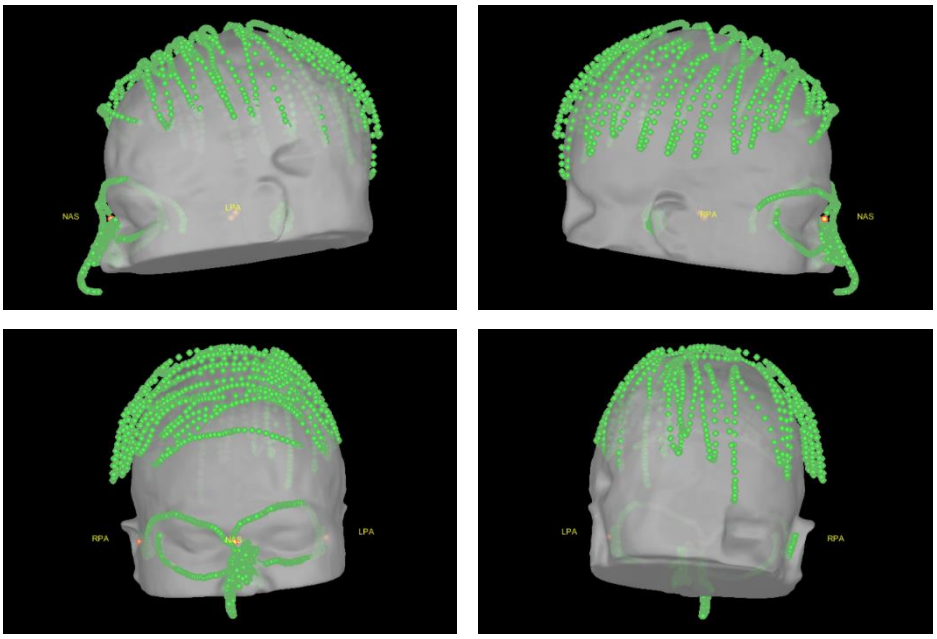

Figure XI-3| Co-registration results obtained with the chamfer based Brainstorm process for Subject A. The anatomical landmarks are labellled in the images (NAS: nasion, RPA: right pre-auricular point, LPA: left pre-auricular point). The recorded points do not fit the skin surface on the right side of the head.

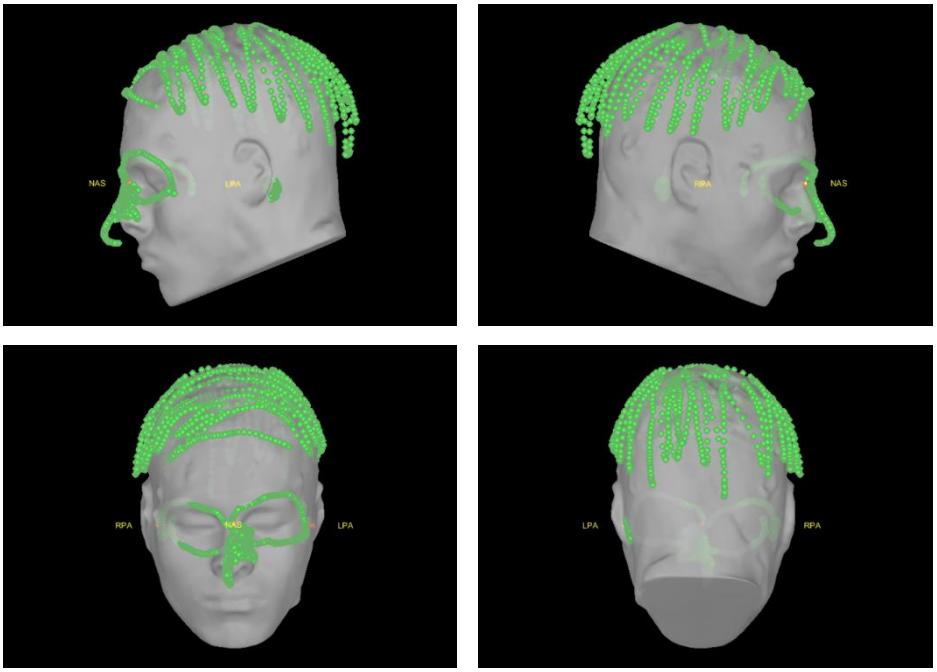

Figure XI-4| Co-registration results obtained with the chamfer based Brainstorm process for Subject B. The anatomical landmarks are labellled in the images (NAS: nasion, RPA: right pre-auricular point, LPA: left pre-auricular point). The recorded points do not fit the skin surface in the occipital region of the head.

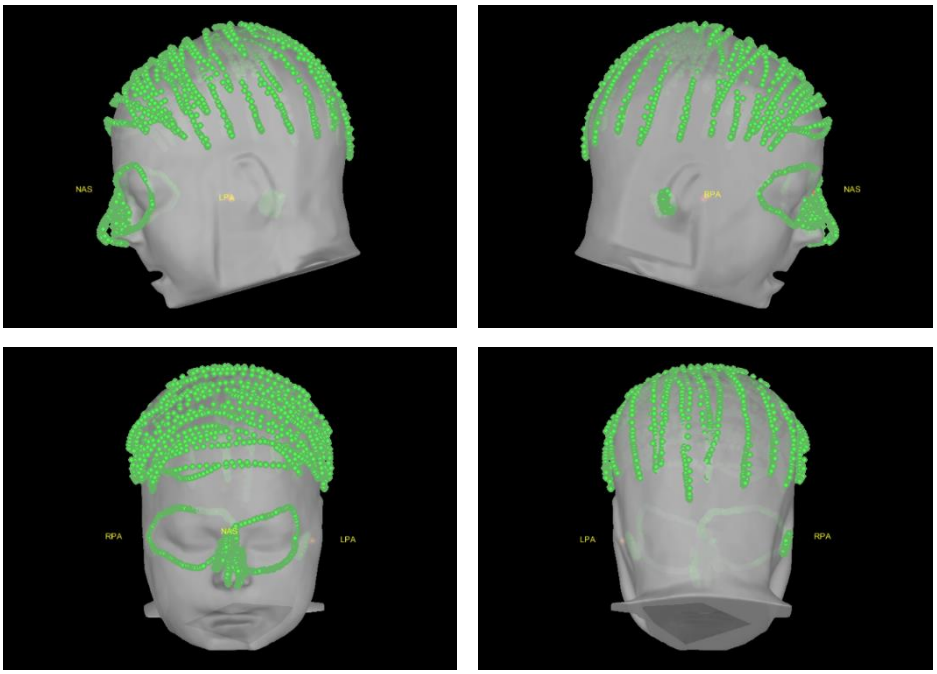

Figure XI-5| Co-registration results obtained with the chamfer based Brainstorm process for Subject C. The anatomical landmarks are labellled in the images (NAS: nasion, RPA: right pre-auricular point, LPA: left pre-auricular point). The process aligned the individual head points properly to the head surface.

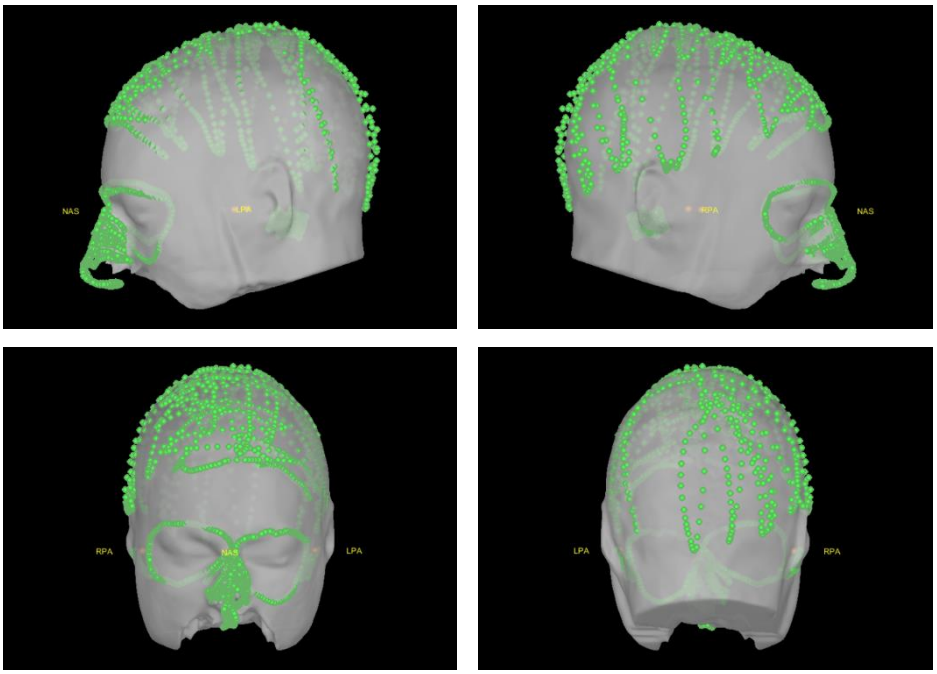

Figure XI-6| Co-registration results obtained with the chamfer based Brainstorm process for Subject D. The anatomical landmarks are labellled in the images (NAS: nasion, RPA: right pre-auricular point, LPA: left pre-auricular point). For the most part the recorded points fit the skin surface, but the 3D point cloud might be tilted slightly to the left.

XII. Discussion

A precise co-registration of functional EEG/MEG data and an anatomical MRI is crucial in order to construct an individual head model which provides the tissue geometries and conductivities for source analyses (head modelling). These head models are needed to determine a dipole position within the subject's brain with a high spatial resolution.

The presented process can be used to align functional data with MR recordings of a given subject. The simulated study showed that the process produces reasonable results, although they were not as good as those achieved by the standard implementation in Brainstorm. Nevertheless, it is obvious that the results became more similar as the noise level of the simulated head points increased. For this reason, it might be investigated if the co-registration based on the chamfer distance map is more stable for noisy data than the Brainstorm process. It should be taken into account that the simulated EEG electrode positions described a more or less hemispherical shape. Therefore, it is possible that the simulated head shape is shifted around the z-axis, since no prominent anatomical markers are included in the simulated head shape. For this reason, the analysis of the real study data was an important point. It is visible that the head points, which include the region around the nose and the eyes, are important in achieving reasonable results. Julie Verreault [Verreault2012] reported that those regions were not co-registered properly to the skin surface. This error was fixed, after the Powell algorithm had been replaced by a simplex algorithm for the minimization procedure. But the co-registration of the skin surface and the recorded head points is influenced by deformations of the 3D point cloud. This is visible in figures 12 and 13. It is obvious that the recorded point clouds for Subject A and B are deformed in some regions. Those deformations might be caused by movements of the reference or during the recording process, for example, if the stylus, which is used by the operator to record the points, does not touch the subject's skin during the recording procedure.

XIII. Conclusion and Outlook

Up to this point, the implemented process generates reasonable results for real study data. It might be used as an alternative procedure, if the original Brainstorm co-registration algorithm does no achieve the desired results. Nevertheless, there are some steps which are crucial in order to improve the chamfer based co-registration process. Basically, four aspects which might need to be improved were found during the process evaluation. Three of them are related to the minimization procedure and the cost function calculation.

The search grid or, more precisely, the number and distribution of the starting points for the minimization algorithm could be improved. With respect to the mean error of the recorded head points and expected head movements or point cloud deformations, an advanced search grid should be defined. For the given search grid, the starting points were rotated around the z-axis only. Since the anatomical markers are defined within the z pane, it was expected that the point cloud is mostly rotated around this axis, while the other ones are fixed. This assumption should be reviewed, before a new search grid is defined. Moreover, it might be useful to refine grid resolution (start with coarse grid and refine it around the best starting point), instead of using random starting points for the second minimization step.

Another approach might be to modify the cost function. For now, the square mean distance is minimized, to achieve the best co-registration. This has been reported as a stable and fast method [Schwartz1996]. However, other cost functions might be evaluated as well, since Schwartz et al. used the Powell algorithm instead of the simplex algorithm. Furthermore, the function `GetCostPO()`, which is used to calculate the cost value, approximates head radius with 0.07 m. The head radius is needed to transform the rotation parameter from mm to angle size. Therefore, a wrong value might cause an inaccurate rotation parameter and erroneous co-registration result.

On a final note, the results for the real study data showed that a correct co-registration is barely possible if the recorded head shape is deformed. For this reason, an additional module or function could be included in the process, to smooth the head shape and remove some noise from the recorded point cloud.

XIV. Appendix II

XIV.I *List of references*

[Borgefors1986] Borgefors, G. *Distance Transformations in Digital Images.* Computer Vision, Graphics and Image Processing, 1986, 34:344-371

[Schwartz1996] Schwartz, D.; Lemoine, D.; Poiseau, E. and Barillot C., *Registration of MEG/EEG data with 3D MRI: Methodology and precision issues*, Brain Topography, Vol. 9, No. 2, 1996.

[Tadel2011] Tadel F, Baillet S, Mosher JC, Pantazis D, Leahy RM, "Brainstorm: A User-Friendly Application for MEG/EEG Analysis," Computational Intelligence and Neuroscience, vol. 2011, Article ID 879716, 13 pages, 2011. DOI:10.1155/2011/879716

[Verreault2012] Verreault, J. *Conception et intégration du module de recalage dans Brainstorm.* École de technologie supérieure, 2012.

XIV.II *List of Figures*

XIV.III *Tutorial: Process AlignChamferDistance*

Sometimes the sensors (electrodes, magnetometers or gradiometers) cannot be aligned properly with the MRI and the surfaces of the subject if the standard co-registration procedure is used.

In this tutorial, we will align the sensors on the subject's head, using the chamfer distance. For this purpose, it is crucial to run a process. This tutorial explains how to select the necessary files and run the process.

Auditory dataset

The dataset used in this tutorial is the same as the one used in the introduction tutorials and in the MEG Auditory tutorial.

License

This tutorial dataset (MEG and MRI data) remains a property of the MEG Lab, McConnell Brain Imaging Center, Montreal Neurological Institute, McGill University, Canada. Its use and transfer outside the Brainstorm tutorial, e.g. for research purposes, is prohibited without written consent from the MEG Lab.

If you reference this dataset in your publications, please acknowledge its authors (Elizabeth Bock, Peter Donhauser, Francois Tadel and Sylvain Baillet) and cite Brainstorm as indicated on the website. For questions, please contact us through the forum.

Place process function in your user folder

The Brainstorm plug-in, or "process" is automatically identified and added to the menus in the pipeline editor, after you placed it in your user folder:

- **$HOME/.brainstorm/process**

Select files to process

For this tutorial we have not used the automatic head shape registration which is executed when you choose the option "**Refine registration with head points**". Instead we will use the chamfer distance to improve the registration between the MRI and the MEG/EEG sensors. The right picture represents the initial NAS/LPA/RPA registration.

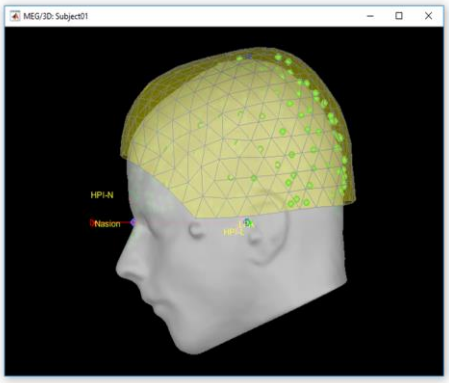

Drag the functional data you want to realign to the subject's MRI in Process1. Make sure that your data contain channel positions or a head shape file, an individual MRI and segmented head surface for the given subject.

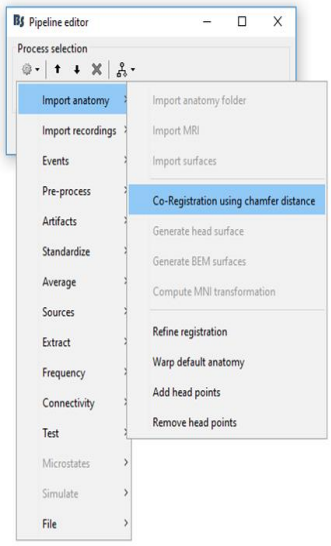

Select process

- Click on the **[Run]** button at the bottom-left corner of the Process1 tab.
- The **Pipeline editor** window appears. Select " Import anatomy > Co-Registration using chamfer distance "

When you have selected the process, the process starts by calculating the chamfer distance matrix.

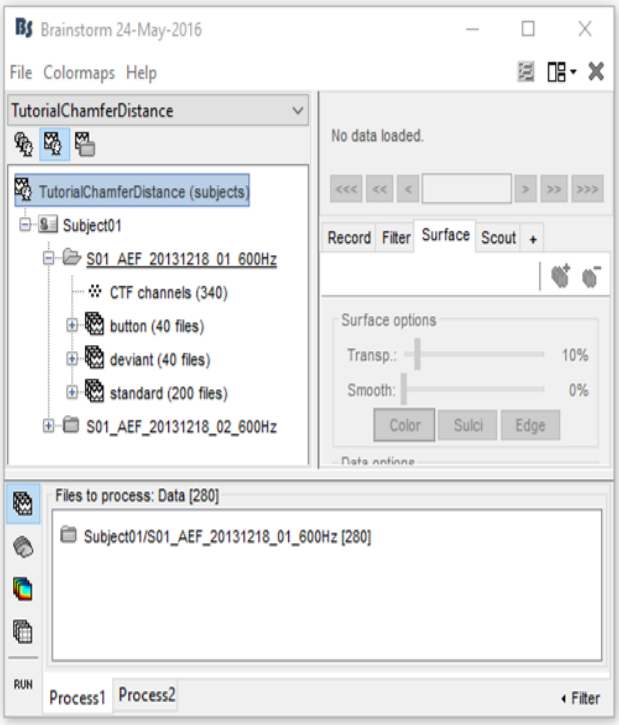

Validation

In the end, the chamfer matrix (note that you might need to adjust the amplitude and the transparency in the surface data options) as well as the registration results are depicted, and the new channel file will be saved in the Brainstorm database. Moreover, the chamfer distance map and the calculated skin surface will be added to the Brainstorm database for the subject.

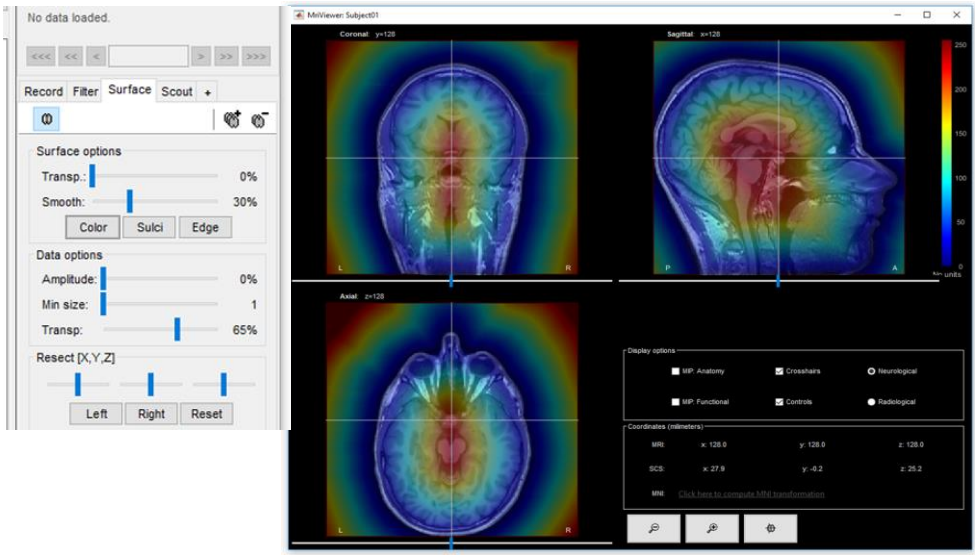

Final registration

The following pictures represent the initial NAS/LPA/RPA registration (top), and the registration based on the chamfer distance (bottom).

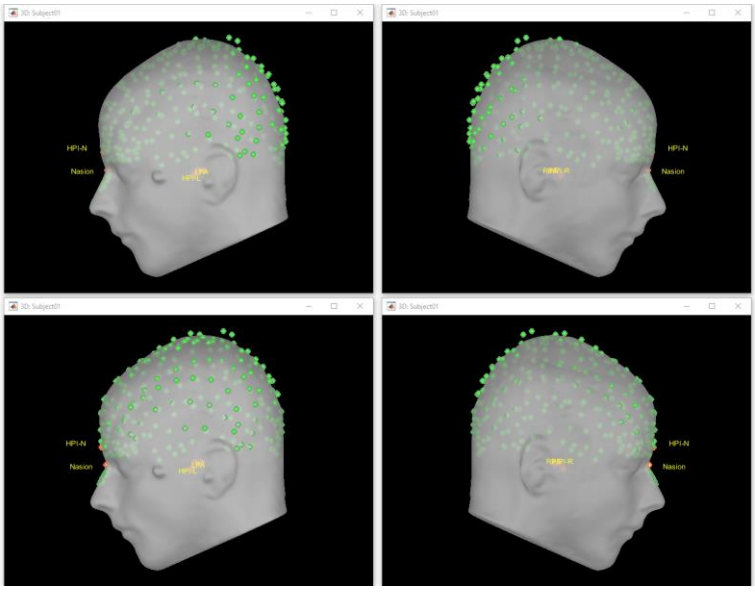

July 11th, 2016

Authorization for Marie Theiss to include her internship report in her MSc. Thesis

Prof. Dr. Heinrich Brinck
August-Schmidt-Ring
10 45665 Recklinghausen

Dear Prof. Dr. Brinck,

With this letter, I authorize Marie Theiss, who did an internship in my laboratory, to include her work and report done during this internship as part of her Master Thesis. Marie arrived in my laboratory, the multimodal functional imaging lab (located both in Physics dpt at Concordia University and in Biomedical Engineering dpt at McGill University, Montreal, Canada) for a period of 3 months from April to June 2016. The project of her internship in my lab was entitled ***"Implementation of a Brainstorm Process for Chamfer Distance based MEG - MRI Co-Registration".*** Her project consisting in adapting to Brainstorm software (a widely recognized software dedicated for Electro-EncephaloGraphy EEG and Magneto-EncphaloGraphy MEG data analysis and source localization), a MEG-MRI automatic co-registration method, based on the study proposed originally published by Schwartz et al 1996, and re-implemented in my lab. The method basically consists in transforming an anatomical MRI of the head into a volumetric distance map from the skin surface (using the so-called Chamfer distance transform method), in order to automatically co-registration a cloud of point digitized from the head of the subject (headshape) to his anatomical MRI. Reaching accurate MEG-MRI co-registration is absolutely crucial to ensure sufficient accuracy of source localization techniques aiming at converting scalp EEG-MEG measurements into current density maps along the cortical surface. Marie did an excellent work and I authorize her to include this report as pert of her Master thesis.

Feel free to contact me directly in case you would like any further information,

Sincerely,

Christophe Grova Ph.D
Assistant Professor, Physics Dpt, Concordia University
PERFORM centre, Chair of PERFORM Applied BioImaging Committee, Concordia University
Adjunct Prof in Biomedical Eng., and Neurology and Neurosurgery Dpt, McGill Univ.
Director of the Multimodal Functional Imaging Lab (Multi FunkIm)
Montreal Neurological Institute - epilepsy group
Email : christophe.grova@concordia.ca
Phone : (514) 848-2424 ext 4221

July 11th, 2016

Reference Letter for Marie Theiss

To whom it may concern,

I am pleased to write this letter to recommend fully the work of Marie Theiss, especially in the context of her finishing her Master of Science and applying for PhD positions. Marie contacted during the year of 2015 in order to come to my lab. for a summer internship, while she was finishing a Master of Science in Molecular Biology from Westphalian University of Applied Science (Recklinghausen, Germany). She arrived in my laboratory, the multimodal functional imaging lab (located both in Physics dpt at Concordia University and in Biomedical Engineering dpt at McGill University, Montreal, Canada) for a period of 3 months from April to June 2016. The project of her internship in my lab was entitled ***"Implementation of a Brainstorm Process for Chamfer Distance based MEG - MRI Co-Registration".*** Her project consisting in adapting to Brainstorm software (a widely recognized software dedicated for Electro-EncephaloGraphy EEG and Magneto-EncphaloGraphy MEG data analysis and source localization), a MEG-MRI automatic co-registration method, based on the study proposed originally published by Schwartz et al 1996, and re-implemented in my lab. The method basically consists in transforming an anatomical MRI of the head into a volumetric distance map from the skin surface (using the so-called Chamfer distance transform method), in order to automatically co-registration a cloud of point digitized from the head of the subject (headshape) to his anatomical MRI. Reaching accurate MEG-MRI co-registration is absolutely crucial to ensure sufficient accuracy of source localization techniques aiming at converting scalp EEG-MEG measurements into current density maps along the cortical surface.

I have been very pleased and impressed by the work Marie completed in such a short period of time (3 months). She has been able to fully understand and follow the code written by someone else, to adapt and re-implement it within the framework of Brainstorm software, by following the guidelines provided by the main developer in charge of Brainstorm project, François Tadel. She also significantly optimized and improved the overall procedure (from a duration of around 20min to 2-3min). Finally at the end of her internship, she provided some preliminary evaluation of the method on simulated data and real data. During her internship, I had several occasions to evaluate that Marie had indeed excellent knowledge of the research field she is working on. She also demonstrated excellent productivity, some independence and was also able to take some interesting initiatives. I asked Marie to give two oral presentations of her work, one in the context of a lab meeting and one with François Tadel and finally she wrote a small report of

the work she did during these 3 months internship in my lab. So I can also certify that she has excellent writing and speaking skills in English. She is overall a brilliant, motivated and very nice person to work with, who well integrated herself within the team and was able to show significant productivity for the short period of time she has been with us.

In conclusion, I am confident that Marie Theiss has all the required expertise and capacity to continue in a very productive PhD program and I therefore fully recommend any of her application. Feel free to contact me directly in case you would like any further information,

Sincerely,

Christophe Grova Ph.D
Assistant Professor, Physics Dpt, Concordia University
PERFORM centre, Chair of PERFORM Applied BioImaging Committee, Concordia University
Adjunct Prof in Biomedical Eng., and Neurology and Neurosurgery Dpt, McGill Univ.
Director of the Multimodal Functional Imaging Lab (Multi FunkIm)
Montreal Neurological Institute - epilepsy group
Email : christophe.grova@concordia.ca
Phone : (514) 848-2424 ext 4221